

UCSF

UC San Francisco Electronic Theses and Dissertations

Title

Polymer Thin Film Devices for Controlled Drug Delivery

Permalink

<https://escholarship.org/uc/item/8k18d5z0>

Author

Lance, Kevin David

Publication Date

2015

Peer reviewed|Thesis/dissertation

Polymer Thin Film Devices for Controlled Drug Delivery

by

Kevin David Lance

DISSERTATION

Submitted in partial satisfaction of the requirements for the degree of

DOCTOR OF PHILOSOPHY

in

Bioengineering

in the

GRADUATE DIVISION

of the

UNIVERSITY OF CALIFORNIA, SAN FRANCISCO

Copyright © 2015

by

Kevin David Lance

Acknowledgements

Elements of this dissertation have been published elsewhere or are in preparation for submission to a peer-reviewed journal. Chapter 2 has been accepted for publication by the journal IOVS under the title “In Vitro and In Vivo Sustained Zero-Order Delivery of Rapamycin (Sirolimus) from a Biodegradable Intraocular Device” by KD Lance, SD Good, et al. Chapter 3 is in preparation for submission to a peer-reviewed journal for publication, and Chapter 4 is in the submission process for publication in a peer-reviewed journal.

This dissertation is the product of a long journey in science that began before my first day of school, and is culminating with this dissertation just little over 22 years of schooling later. I have many people to thank, but first and foremost have to thank my family for everything. If it hadn't been for all that Lego building I did at the beginning, I never would've ended up building drug delivery devices many years later.

My deep dive into science began with my high school biology teacher, Linda Wichers, and physics teacher, Doug Baltz, and they are responsible for showing me all that there is to discover in the world of science. I also have to thank my robotics teacher, Bernie Sims, who taught me some of the first machine shop techniques that I'm still using years later.

I have a slew of scientific mentors that I have to thank for the opportunities they've given me and the lessons they've taught me in the many labs I've been in. At the University of Michigan I was lucky enough to get my start in the lab of Michael Mayer, who I thank for his patience and ability to mentor students into independent thinkers and doers in lab. Chuck Burant and Raoul Kopelman also welcomed me into their labs and helped me learn the skills and patience I would need in need later on in graduate school. During my six months at Merck I was

also lucky to learn from Dicky Abraham, Sean Baker, and Serena Fries Smith, who all taught me how to be a better scientist, communicator, and labmate.

At Berkeley and UCSF I've found more mentors to help guide my journey. Bob Bhisitkul, Dorian Liepmann, and Zev Gartner have all helped me figure out my way on the path in front of me, whether it was during graduate school or beyond. Tejal Desai has been a fantastic research mentor and I've always admired her ability to lead a lab built of so many different personalities in so many projects while balancing it all with a life outside of the lab. Without Tejal guiding me, graduate school would've been a much more difficult journey.

My friends have always been a source of encouragement and support, and I'm lucky I have many great ones. I have to thank Kat Montgomery for always having the time to lend an ear when things got tough. I also have to thank James Pinney, Alec Cerchiari, Matt Rubashkin, and Todd Duncombe for all the fun and inspiring happy hour debates we've had during graduate school.

Lastly, but most importantly, I want to thank my first and only wife Shea for chasing me across the country to the Bay Area. I'm a lucky guy to get your love and support and I couldn't have done any of this without you.

Polymer Thin Film Devices for Controlled Drug Delivery

Kevin David Lance

Abstract

This dissertation covers the use of several types of polymer thin films for sustained drug delivery in the back of the eye (BOTE) and the peripheral vasculature. In general, the thin films are combined around a drug payload to restrict its release into the surrounding *in vitro* or *in vivo* environment. The polymer films make use of micro- and nanotechnology to control the release behavior of the various drugs they encapsulate. All devices aim to enable or extend the delivery of therapeutics to their target site of action.

The first device presented uses polycaprolactone (PCL) thin films to encapsulate rapamycin. The device achieves sustained release of rapamycin to the retina, while also possessing the ability to modulate release of the drug by changing the thickness of the films.

A second drug delivery device here presented uses nanoporous PCL thin films to control the release of the large molecule therapeutic ranibizumab from the device. The nanopores of this PCL device work to restrict the diffusion of the drug through the films and results in a detectable concentration of ranibizumab in the vitreous up to 12 weeks.

The third device type described here uses varying compositions of PLGA films to achieve unidirectional, sustained, and local release of the specialized pro-resolving mediator RvD1 for surgical applications. The thin film layers of PLGA are combined to create a drug-

eluting wrap that can be wrapped around sites of vascular surgery to limit post-surgical inflammation.

These demonstrations illustrate the diverse therapeutic areas where biodegradable polymer thin films may improve pharmacokinetics, patient quality of life, and overall outcomes. Across the spectrum of small to large molecules and the many target site for drug delivery in the body, polymer thin films can be used in a variety of advanced devices to solve the challenges of medicine.

Table of Contents

ACKNOWLEDGEMENTS	iii
ABSTRACT	v
LIST OF FIGURES	xii
LIST OF TABLES	xiv
CHAPTER 1 – Introduction.....	1
CHAPTER 2 – In Vitro and In Vivo Sustained Zero-Order Delivery of Rapamycin (Sirolimus) from a Biodegradable Intraocular Device	9
2.1 Abstract	10
2.2 Introduction.....	10
2.3 Material and methods.....	13
2.3.1 Materials	13
2.3.2 Film fabrication.....	13
2.3.3 Device fabrication	14
2.3.4 In vitro release experiments and analysis	14
2.3.5 Adsorption release and powder x-ray diffraction (PXRD)	15
2.3.6 In vivo experiments and analysis	15

2.4 Results.....	17
2.4.1 Rapamycin release from 16 mm devices and bulk films	17
2.4.2 Rapamycin release from 6 mm devices	18
2.4.3 Adsorption release and powder x-ray diffraction (PXRD).....	19
2.4.4 In vivo rapamycin pharmacokinetics	19
2.5 Discussion	20
2.6 Conclusions.....	24
2.7 Acknowledgements.....	24
CHAPTER 3 – In Vivo and In Vitro Sustained Release of Ranibizumab from a Nanoporous Thin Film Device.....	36
3.1 Abstract.....	37
3.2 Introduction.....	37
3.3 Materials and Methods.....	40
3.3.1 Materials	40
3.3.2 FITC-Ranibizumab Preparation.....	41
3.3.3 Device Fabrication.....	41
3.3.4 Scanning Electron Microscopy	42

3.3.5 In vitro Elution Experiments.....	42
3.3.6 In vivo Elution Experiments	43
3.3.7 Post in vivo Elution Experiments and Scanning Electron Microscopy	43
3.3.8 High Performance Size Exclusion Chromatography (HPSEC).....	44
3.3.9 Quartz Crystal Microbalance (QCM)	44
3.4 Results.....	45
3.4.1 Device Morphology	45
3.4.2 In vitro FITC-Ranibizumab Release.....	45
3.4.3 In vivo FITC-Ranibizumab Release	46
3.4.4 In vivo Safety Profile.....	47
3.4.5 Drug Stability and Protein Adsorption	47
3.5 Discussion.....	48
3.6 Conclusion	51
3.7 Acknowledgements.....	52
CHAPTER 4 – Unidirectional and Sustained Delivery of the Pro-Resolving Lipid Mediator Resolvin D1 from a Biodegradable Thin Film Device	60
4.1 Abstract.....	61

4.2 Introduction.....	61
4.3 Material and Methods	63
4.3.1 Materials	63
4.3.2 Device Fabrication.....	64
4.3.3 In vitro Elution Experiments.....	65
4.3.4 In vitro Directional Elution Experiments.....	65
4.3.5 Liquid Chromatography-Tandem Mass Spectrometry	65
4.3.6 In vitro Bioassay Experiments.....	66
4.3.6.1 NF- κ B Assay (p65 Nuclear Translocation)	67
4.3.6.2 Cell Proliferation Assay	67
4.3.6.3 Migration Assays	68
4.3.6.4 MTT Assay	68
4.3.7 Ex vivo Flow Chamber for Vascular Delivery	68
4.3.8 In vivo Drug Delivery Models.....	69
4.4 Results.....	70
4.4.1 Device Morphology	70
4.4.2 In vitro RvD1 Release from Devices.....	71

4.4.3 Directional in vitro RvD1 Release.....	73
4.4.4 Assessment of RvD1 Release and Stability by LC-MS/MS.....	73
4.4.5 In vitro Biological Assays with RvD1 Eluting Trilayered Devices.....	73
4.4.6 Ex vivo and in vivo Delivery of RvD1	74
4.5 Discussion.....	75
4.6 Conclusions.....	79
4.7 Acknowledgements.....	79
CHAPTER 5 – Summary and Conclusions	97
REFERENCES.....	100

List of Figures

Figure 1.1. Relative pharmacokinetics of delivery methods.....	5
Figure 1.2. Atomic structure of PLGA and PCL	6
Figure 1.3. Fundus photograph of age-related macular degeneration.....	7
Figure 1.4. Anatomy of the eye highlighting the uvea.....	8
Figure 2.1. First generation rapamycin devices and release	26
Figure 2.2. Second generation rapamycin devices and release	27
Figure 2.3. HPLC trace of rapamycin and seco-rapamycin	28
Figure 2.4. Cell proliferation assay for fresh and extracted rapamycin	29
Figure 2.5. Adsorption, elution, and PXRD of rapamycin.....	30
Figure 2.6. In vivo pharmacokinetics of rapamycin	32
Figure 2.7. In vivo device location and safety	34
Figure 2.8. Residual drug payloads for in vivo devices.....	35
Figure 3.1. Fabrication and morphology of nanoporous devices.....	53
Figure 3.2. In vitro release behavior of nanoporous devices	54
Figure 3.3. In vivo behavior of nanoporous devices.....	55
Figure 3.4. Nanoporous device in vivo safety	57
Figure 3.5. FITC-ranibizumab stability and adsorption.....	58

Figure 3.6. Stability analysis of native Lucentis.....	59
Figure 4.1. Assembly and elution characteristics of PLGA devices.....	81
Figure 4.2. Mass change and morphology change of trilayered devices	83
Figure 4.3. Directional release of RvD1 from trilayered devices	84
Figure 4.4. Identification and quantification of RvD1 released from devices	85
Figure 4.5. Biological activity of release RvD1.....	87
Figure 4.6. Translocation of p65 from exposure to RvD1 devices	89
Figure 4.7. Endothelial scratch closure with an RvD1 device	91
Figure 4.8. MTT cytotoxicity with RvD1 devices	92
Figure 4.9. Assay standard curve for RvD1 tissue detection.....	93
Figure 4.10. Unidirectional in vivo release of RvD1	94
Figure 4.11. Ex vivo flow chamber setup	96

List of Tables

Table 2.1 Concentration values for in vivo rapamycin release	33
--	----

Chapter 1 – Introduction

The field of controlled drug delivery spans a variety of methods by which the pharmacokinetics of delivering therapeutics to the body are changed in order to improve outcomes. Traditional drug delivery, such as injections or oral dosing with a pill, is able to create a drug concentration in the body within the therapeutic window where drugs are safe and effective. However, traditional drug delivery can also necessitate concentrations that spike above the upper therapeutic concentration limit, where toxicity is a concern, and will ultimately fall below the lower therapeutic concentration limit where the drug is no longer effective (Figure 1.1).

Controlled drug delivery methods can release drug in a sustained manner over long periods of time so that the upper limit of the therapeutic window is not breached, while also maintaining concentrations about the lower limit of the therapeutic window. The goal of the controlled drug delivery described in this dissertation is to create drug delivery devices capable of the sustained release of drugs for an extended period of time relative to traditional drug delivery methods. The therapeutics covered in this dissertation and for treatment of neovascular age-related macular degeneration, chronic uveitis, and inflammation.

1.1 Biodegradable Polymers and Thin Films

The biodegradable polyesters polycaprolactone (PCL) and poly(lactic-co-glycolic) acid (PLGA) (Figure 1.2) are common polymers used in the field of drug delivery. In this dissertation, both polymers are used for their ability to be cast as thin films (5-30 μm) that can be fabricated into drug delivery devices.

PCL is a polyester frequently used for drug delivery and tissue engineering owing to its adaptability to many delivery systems, its generally well-tolerated biocompatibility, and its slow degradation behavior on the order of months to years.¹ Previous work with PCL has shown it can be made microporous and nanoporous as a means of controlling drug delivery, and macroscopic film devices made of PCL are well tolerated in the posterior chamber of the eye.²⁻⁴

Akin to PCL, PLGA is also a biodegradable polyester that is commonly used in the field of controlled drug delivery.⁵ Although most commonly used as a micro- or nanoparticle, in this dissertation it is fabricated as a thin film to create a biodegradable, drug-eluting wrap. PLGA demonstrates a range of degradation times, depending on the ratio of lactide to glycolide monomers chosen to compose the PLGA polymer chain, as well as the geometry of the final PLGA construct.^{6,7}

1.2 Neovascular Age-Related Macular Degeneration and Current Treatments

Age-related macular degeneration (AMD) is a disease whose symptoms usually begin with gaps or distortion in vision and leads to gradual loss of central vision, and can ultimately lead to blindness.⁸ Neovascular AMD is one of two types of AMD. In neovascular AMD, abnormal blood vessel growth occurs underneath the retina and can lead to the hemorrhaging of fluid and the detachment of the retina (Figure 1.3), often causing the first symptoms of neovascular AMD.⁹

Current treatment of neovascular AMD uses VEGF binding agents to inhibit the development of neovascularization and vascular leakage.¹⁰⁻¹² Ranibizumab is the antigen-binding fragment of a humanized VEGF-binding antibody frequently used in the treatment of

neovascular AMD by means of intravitreal injection on a roughly monthly basis.^{10,13-15} In this dissertation we aim to improve upon the delivery of ranibizumab by injection by means of an implantable reservoir devices capable of releasing ranibizumab in a sustained manner.

1.3 Uveitis and Current Treatments

Uveitis is a cause of blindness that may represent up to 10% of legal blindness in developed countries and occurs mostly between 20 and 60 years of age.^{16,17} Uveitis is defined by inflammation of the iris, ciliary body, and/or choroid (Figure 1.4) and though infection is a main cause, uveitis can have an unknown or non-infectious etiology. Non-infectious uveitis is treated with immunosuppressants if the disease is non-responsive to corticosteroids, if inflammation recurs, or if systemic side effects are too severe.¹⁸ With uveitis, local delivery of therapeutics is especially attractive given the ease of access to the eye and the severe side effects uveitis treatments can create when given systemically.¹⁹

Rapamycin (sirolimus) is a macrolide immunosuppressive drug that can produce severe side effects if given orally, but is being investigated as a local treatment for uveitis when dosed as a bimonthly intravitreal injection.²⁰ Importantly, local dosing of rapamycin shows systemic concentrations of rapamycin below the dose necessary for systemic side effects to occur. In this dissertation we present it as a candidate for local delivery to the posterior chamber of the eye from a long-term, sustained release drug delivery device to avoid the problems associated with repeated dosing by injection for chronic uveitis.

1.4 RvD1 for the Resolution of Inflammation

Resolvin D1 (7S,8R,17S-trihydroxy-4Z,9E,11E,13Z,15E,19Z-docosahexaenoic acid; RvD1) is a specialized pro-resolving mediator (SPM) that promotes the resolution of inflammation.²¹ As one application, the introduction of RvD1 following surgical intervention on the peripheral vasculature can attenuate vascular smooth muscle cell activation and neointimal hyperplasia.^{22,23} However, current techniques to administer SPM therapeutics rely on intravenous, intraperitoneal, and intra-arterial delivery which do not allow for local delivery of SPMs and may offer inferior pharmacokinetics to a local drug delivery device.

Perivascular wraps fabricated from thin films of PLGA are an attractive local delivery system for SPMs due to their flexibility, easy tissue adherence, and degradation behavior on the same timescale as the wound healing response.^{5,6,24} In this dissertation, we develop a multilayered PLGA thin film perivascular wrap capable of the sustained and unidirectional release of the SPM therapeutic RvD1.

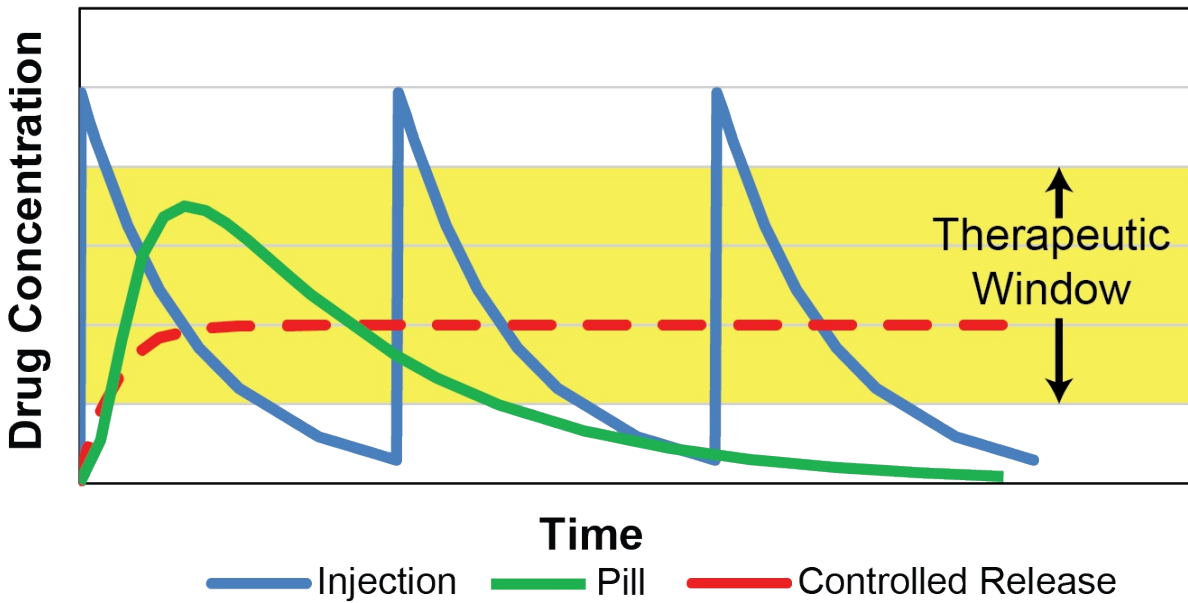


Figure 1.1 Relative pharmacokinetics of traditional injections, traditional pills, and controlled release. Controlled release methods remain in the therapeutic window where drugs are effective for longer periods of time than other dosing methods.

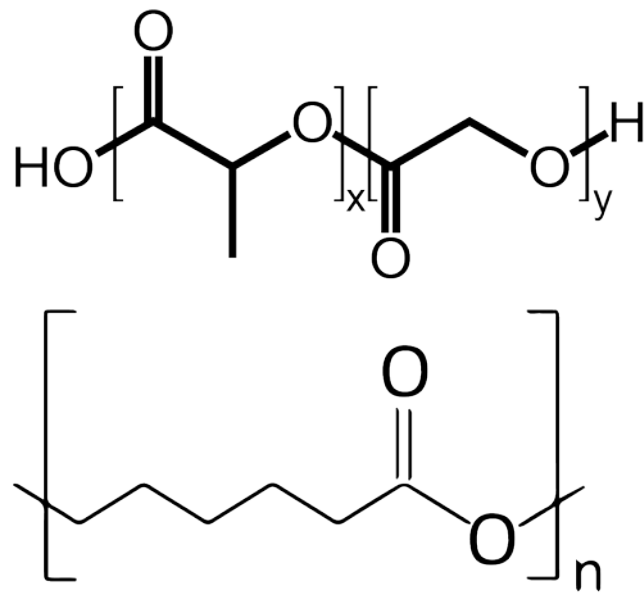


Figure 1.2 Atomic structure of PLGA (top) and PCL (bottom). For PLGA, X and Y denote the segments of lactide and glycolide, respectively.



Figure 1.3 A fundus photograph showing advanced age-related macular degeneration in the back of the eye. The darker central portion is a hemorrhage. Image courtesy of the National Eye Institute, National Institutes of Health.

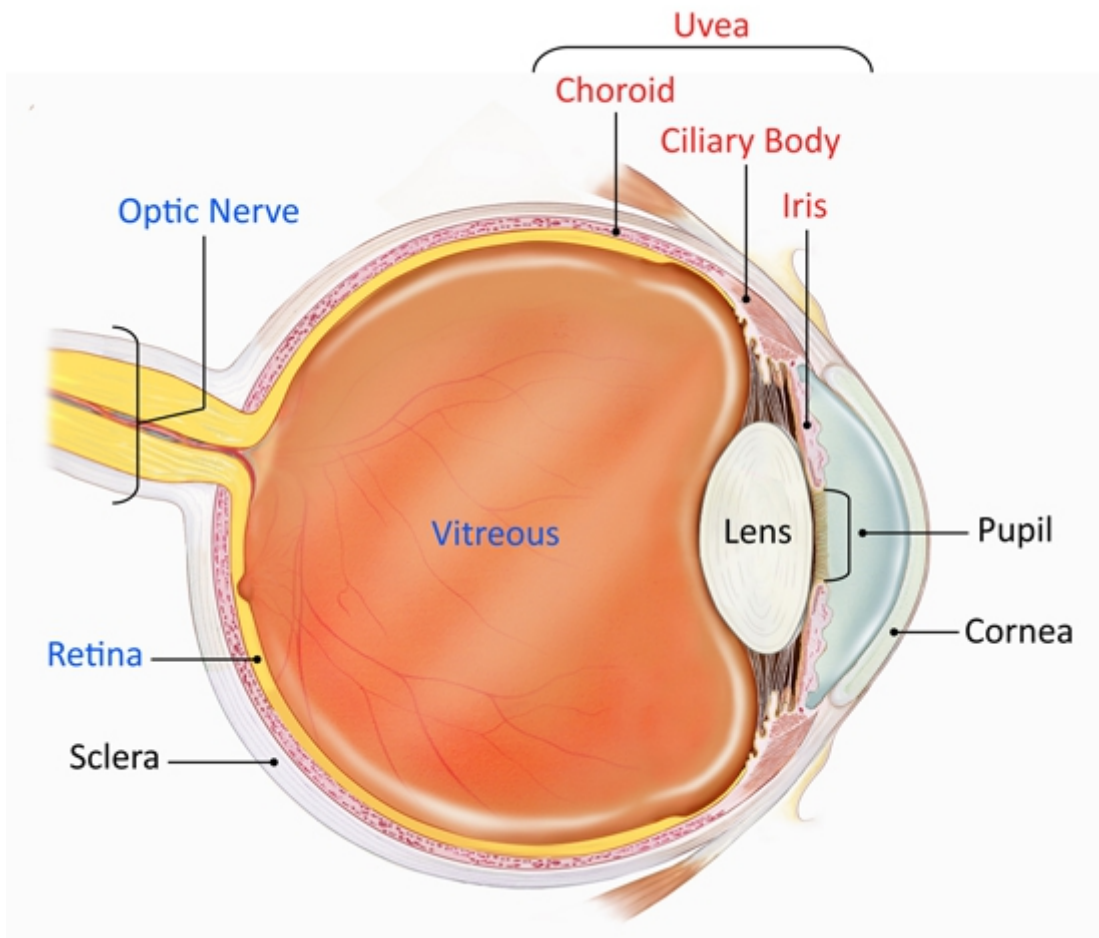


Figure 1.4 Anatomy of the eye highlighting the uvea and the three tissues susceptible to uveitis. Image courtesy of the National Eye Institute, National Institutes of Health.

Chapter 2 - In Vitro and In Vivo Sustained Zero-Order Delivery of Rapamycin (Sirolimus) from a Biodegradable Intraocular Device

2.1 Abstract

Rapamycin is a potent immunosuppressant under investigation for bimonthly intraocular administration for the treatment of uveitis. Polycaprolactone thin films were used to encapsulate rapamycin to create implantable intraocular devices capable of zero-order drug release over the course of months. In vitro release of rapamycin was observed to be zero-order through 14 weeks of study. Release rates were tunable by altering PCL film porosity and thickness. In vivo release of rapamycin was observed out through 16 weeks with concentrations in the retina-choroid in the therapeutic range. Rapamycin concentration in the blood was below the lower limit of quantification. The drug remaining in the device was found to be chemically stable both in vitro and in vivo and was sufficient to last for upwards of 2 years of total release.

2.2 Introduction

Uveitis is a significant cause of blindness characterized by inflammation in the anterior, intermediate, and/or posterior uvea or retina of the eye, with posterior uveitis as the most challenging to treat. Non-infectious uveitis is often treated first with corticosteroids but is followed by immunosuppressants if corticosteroids fail to control inflammation, if inflammation reoccurs despite corticosteroid use, or if systemic side effects occur.¹⁸

Rapamycin (also known as sirolimus) is a macrolide drug currently used for immunosuppression in renal transplantation,²⁵ prevention of restenosis by elution from coronary stents,^{26,27} and for the treatment of chronic uveitis.^{28,29} However, the oral administration of rapamycin against uveitis can result in severe side effects, so an alternative delivery method is desirable. Currently, an intraocular injection of a liquid formulation of rapamycin is in clinical

trials for treatment of uveitis.²⁰ The injection is delivered directly into the vitreous, and treatment requires bimonthly injections for the duration of the chronic disease.^{30,31} Intraocular administration of rapamycin in a small cohort of patients demonstrated no significant adverse effects, and levels of rapamycin in the blood were well below the concentration where systemic side effects occur.³⁰ Intraocular administration of rapamycin is a potential route for treatment of posterior uveitis that bypasses the side effects associated with systemic administration. Recent work has explored the use of silicon microparticles for the intravitreal delivery of rapamycin, but release kinetics appear to be limited to approximately one month.^{32,33}

Long-term zero-order release behavior is a goal for drug delivery devices because a constant drug elution rate will equilibrate to a steady-state drug concentration, which can be engineered within the therapeutic window of the drug. In the posterior of the eye, zero-order release offers additional potential benefits in treating chronic diseases which otherwise require repeated drug injections into the eye. In addition, zero-order drug release devices can maximize the effect of small drug payloads imposed by the size limits of the eye. Current administration techniques for rapamycin, such as eye drops³⁴ and injections³⁰, fall short in their ability to achieve sustained drug concentrations in the eye over periods of a month or longer. The importance of long-duration rapamycin delivery is indicated by another mTOR inhibitor, everolimus, which in one study was shown to be effective in refractory uveitis, but uveitis returned in 4 out of 8 patients following the end of everolimus therapy.³⁵ Patient compliance is also a major issue for treatments using eye drops, as one study of compliance in glaucoma patients found improper medication delivery (missing a dose or improper administration) in 53.3% of patients.³⁶ Other drug delivery systems for the treatment of uveitis with corticosteroids

are available, but none are currently approved for the delivery of rapamycin or similar immunosuppressants.^{19,37,38}

Zero-order drug delivery devices implanted intravitreally are one way to improve the amount of time an administered drug resides within the therapeutic window at its ocular site of action. One approach in development for sustained drug release in the eye is a device composed of nanoporous, biodegradable polycaprolactone (PCL) thin films which allow zero-order release of therapeutic proteins through the nanopores.³ PCL is a polyester with a favorable intraocular biocompatibility profile that can be fabricated into thin films with thicknesses in the range of 10-40 μm .^{3,4,39} Additionally, PCL thin films can be patterned with nanofeatures or microfeatures by solvent-casting to modify diffusion behavior through the thin films.² Control of the nano- and microstructure of a PCL thin film allows tuning of drug diffusion behavior across the film. Previous *in vivo* studies on the safety of these PCL thin films has shown them to be well tolerated in the posterior chamber of rabbit eyes over 6 months, in addition to showing minimal changes in morphology from degradation.⁴ Based on previous *in vivo* studies it is estimated that PCL will remain intact for approximately 3 years before losing mechanical integrity.³⁹⁻⁴¹

In this work, we investigate a drug delivery device for rapamycin that demonstrates zero-order release behavior up to 14 weeks *in vitro*. The device is composed of a solid rapamycin pellet encapsulated by two PCL thin films, which can be modified to alter the release profile of the device. *In vivo* results show that the drug is stable in the device, reaches its target tissue at the retina/choroid, and sustains release behavior up to 16 weeks. No systemic adverse effects were observed, and the concentration of rapamycin in the blood was below detection limits.

2.3 Material and methods

2.3.1 Materials

Polycaprolactone (80 kDa M_n), 2,2,2-trifluoroethanol (TFE), and 2kDa M_n polyethylene glycol (PEG) were obtained from Sigma-Aldrich (St. Louis, MO). Rapamycin was obtained from Santen, Ltd. (Osaka, Japan). Phosphate-buffered saline (PBS) was obtained from VWR (Radnor, PA), polyoxyl-40-stearate (also known as polyoxyethylene (40) monostearate, Myrj 52) from Spectrum Chemical (New Brunswick, NJ), seco-rapamycin from Santa Cruz Biotech (Dallas, TX), polydimethylsiloxane (PDMS) from Thermo Fisher Scientific (Waltham, MA), and nichrome wire from Consolidated Electronic Wire and Cable (Franklin Park, IL).

2.3.2 Film fabrication

Polycaprolactone was dissolved in TFE and then spun-cast on a 3-inch silicon wafer to make unfeatured PCL films without porogens. Concentrations of PCL in TFE were varied between 100 mg/mL and 300 mg/mL to change the resulting thickness of the spun-cast film.

Microporous PCL films were made by adding polyethylene glycol at a concentration of 150 mg/mL in solutions of PCL and TFE. Films that were rapamycin-loaded in their bulk were prepared by combining solutions of 5mg/mL rapamycin in TFE with solutions of 150 mg/mL PCL in TFE, or a solution of both PCL and PEG at 150 mg/mL in TFE. PCL film morphology was investigated by scanning electron microscopy (SEM) performed on a Carl Zeiss Ultra 55 FE-SEM.

2.3.3 Device fabrication

Rapamycin-loaded devices were prepared by heat-sealing PCL films around a central rapamycin payload (Figure 2.1A). Two sets of devices were made, one set 16 mm in diameter and another set 6 mm in diameter. Devices 16 mm in diameter encapsulated 0.5-2.0 mg of pure loose rapamycin between two PCL films. No excipient was used. These 16 mm devices were made either with two unfeatured PCL films to create a device without introduced pores, or one microporous and one unfeatured PCL film. The second set of devices were 6 mm in diameter with a pelleted rapamycin disc of mass 1.0-2.5 mg. The drug pellets consisted of pure rapamycin without excipients. Devices 6 mm in diameter were assembled either with two unfeatured PCL films or with one microporous film and one unfeatured PCL film.

Devices were assembled by placing the drug pellet between PCL films atop a PDMS slab with an embedded nichrome wire as a heating element. A PDMS annulus and a weight on top of the device held the films together for sealing. Current passed through the wire heat-seals the circumference of the devices.

2.3.4 In vitro release experiments and analysis

In vitro release experiments were conducted in 2 mL of an elution media of PBS (pH 7.4) with 0.1% (w/v) polyoxyl-40-stearate to increase rapamycin solubility and stability in the elution media. A 2mL elution volume was used as it is approximately the same as the vitreous volume in New Zealand White rabbits (~1.5 mL). Polyoxyl-40-stearate has been shown to improve solubility and stability of rapamycin by approximately a factor of ten.⁴² Polyoxyl-40-stearate was also added to reduce the tendency of rapamycin to adsorb to the surface of tubes used in

elution studies. Devices were incubated in elution media at 37 C with constant shaking on an orbital shaker. Elution media was completely replaced at sampling intervals. Rapamycin concentrations were assayed by UV spectrophotometry at 278 nm. Rapamycin stability in the devices and dissolution media was assayed by HPLC as described previously.⁴³ Release studies were carefully designed with frequent time points to avoid saturation of the elution media with drug. At all time points the signal from drug loaded devices were blanked to empty controls. Linear regressions were calculated using Microsoft Excel (Redmond, WA).

2.3.5 Adsorption release and powder x-ray diffraction (PXRD)

Rapamycin was dissolved in methanol and pipetted onto the surface of PCL films. Rapamycin adsorbed to the PCL thin film after methanol evaporation. For release experiments, rapamycin was dissolved to 10 mg/mL and adsorbed by adding varying volumes of the methanol solution to the films. For release experiments, 1, 2.5, and 5 μ L of solution (10, 25, and 50 μ g of rapamycin) was adsorbed. For PXRD analysis, rapamycin was dissolved to 200 mg/mL and 30 μ L was adsorbed onto PCL thin films.

2.3.6 In vivo experiments and analysis

In vivo release experiments were performed in New Zealand White rabbits for vitreous drug release. Devices 6 mm in diameter with one microporous and one unfeatured PCL film were implanted into the posterior chamber of the right eye under general anesthesia and sterile conditions via a 2 mm scleral incision made circumferentially 2 mm posterior to the limbus using

a 20-gauge MVR blade, then closing the incisions with 7-0 vicryl sutures. The left eye was left as an untreated control. In vivo safety and tolerability were evaluated by monitoring intraocular pressure (IOP), adverse events, and inflammation. Inflammation of the conjunctiva/sclera and surgical insertion site, edema, vitreous leakage, cataract formation, polymer appearance and location, hyphema, retinal detachment, anterior chamber fibrin or cell debris, and vitreous humor change were specifically monitored. IOP was taken with a benchtop pneumotonometer (Model 30 Classic, Mentor O&O, Inc., Norwell, MA, USA) for both eyes.

The study design had two arms. One arm was designed for six rabbits, with animal sacrifice and whole eye collection and dissection for vitreous and ocular tissue samples, 2 animals at each time point of 4, 8, and 16 weeks. A second arm was designed for three rabbits as survival studies, to allow longitudinal pharmacokinetic studies with multiple serial vitreous samples taken from each study eye at weeks 1, 2, 4, 8, and 12 by partial microvitrectomy, with a final sample at week 16 after animal sacrifice. Microvitrectomy was performed in a sterile fashion under anesthesia using the Intrektor (Insight Instruments, Stuart, FL), a 23-gauge sutureless vitreous cutting/aspiration device, entering the sclera 2 mm posterior to the limbus at a site 180° from the thin-film device insertion to collect 100-200 µl of vitreous at each sampling procedure. As planned, rabbits were sacrificed at 4, 8, and 16 weeks with the exception of one sacrifice at day 3 and one sacrifice at week 3 due to complications from non-ocular infections unrelated to the device. The data from the two euthanizations due to complications are included in the results presented.

Rapamycin concentration and stability in the vitreous and the retina-choroid was assayed via LC/MS-MS with positive electrospray ionization in multiple reaction monitoring mode. The lower limit of quantitation for vitreous samples was 0.06 ng/mL, the limit for retina-choroid

samples was 1.06 ng/g, and the limit for whole blood samples was 0.5 ng/mL. The ion transition monitored was 931.6 to 864.6 and tacrolimus was used as an internal standard to control for any loss of rapamycin during purification, most notably due to surface adsorption. Owing to the specificity of LC/MS-MS, the assay is specific to stable rapamycin in the samples tested of the residual drug in the devices and the vitreous.

Data is reported as +/- the standard deviation. Statistics were performed using a Student's t-test with a significance threshold at 0.05. ARVO guidelines for the care and use of laboratory animals according to the ARVO Statement for the Use of Animals in Ophthalmic and Vision Research have been observed.

2.4 Results

2.4.1 Rapamycin release from 16 mm devices and bulk films

Release characteristics of rapamycin devices 16 mm in diameter (Figure 2.1A-C) were tested in vitro and compared against the rapamycin release from films that were bulk-loaded with rapamycin. Figure 2.1D shows the difference in kinetics between rapamycin that has been bulk-loaded throughout a PCL film and rapamycin released from either microporous or unfeatured (without introduced pores) rapamycin devices. When fit by linear regression, microporous devices released 2.92 $\mu\text{g}/\text{day}$ ($R^2 = 0.999$) and unfeatured devices released 2.02 $\mu\text{g}/\text{day}$ ($R^2 = 0.997$). Rapamycin release from a bulk-loaded film was non-linear, though the initial pseudo-linear region up to day 6 shows a release of 16.6 $\mu\text{g}/\text{day}$ ($R^2 = 0.822$).

2.4.2 Rapamycin release from 6 mm devices

A second form factor of device was designed based on enhanced fabrication techniques to result in a 6 mm device containing a pelleted rapamycin payload (Figure 2.2A-B). In vitro release experiments with 6 mm devices (Figure 2.2C) show the release of rapamycin from microporous devices (1.78 mg/day, $R^2 = 0.993$) as nearly identical to the release from rapamycin pellets not contained by a PCL device (1.73 mg/day, $R^2 = 0.987$). Rapamycin released from an unfeatured device shows significantly slower release (0.493 mg/day, $R^2 = 0.978$) while maintaining a zero-order release profile. Release in all device types continued to be zero-order out to 14 weeks, and sufficient payload remained in the devices to release for a further 1.6 years for microporous devices and 4.6 years for unfeatured devices.

The ability of PCL thickness to modulate release kinetics was studied using films constructed of two layers of unfeatured 4 μm , 16 μm , or 66 μm thick PCL. Over 5 weeks devices constructed from 4 μm thick films released 37 mg of rapamycin, while devices of 16 μm and 66 μm thick films released 30 and 22 μg of rapamycin, respectively (Figure 2.2D). The similar release rates of the three thicknesses of device after week two suggest that the impact of PCL film thickness on rapamycin release is focused in the initial two weeks of release. The differences in release during the first two weeks may be attributed to the amount of time rapamycin takes to reach equilibrium across the films of varying PCL thicknesses.

The stability of solid rapamycin in the device was confirmed in vitro by HPLC and human smooth muscle cell (HSMC) proliferation, and in vivo by LC-MS/MS. In vitro 6 mm unfeatured devices were incubated in an elution experiment for 14 weeks and then dissected to remove the solid rapamycin pellet. HPLC performed on the drug pellets (n=3) showed peaks

identical to pure rapamycin and no presence of the primary degradation product seco-rapamycin, nor any other significant peak indicative of degradation (Figure 2.3). Comparing extracted rapamycin to fresh rapamycin prepared from stock showed no difference in its ability to inhibit HSMC proliferation (Figure 2.4). For in vivo quantification, LC-MS/MS was used to detect the presence of intact rapamycin in the device through 16 weeks of implantation and for in vivo vitreous samples.

2.4.3 Adsorption release and powder x-ray diffraction (PXRD)

Rapamycin adsorbed to a surface showed an initial burst release followed by slower sustained release out to 3 days (Figure 2.5A). Rapamycin pellets in the same in vitro experiment demonstrated zero-order release which continued past 3 days, and demonstrated a much longer potential release in other in vitro experiments. To examine drug crystallinity, PXRD was performed both on rapamycin powder and on rapamycin adsorbed to the surface of unfeatured PCL films. The results (Figure 2.5B) show characteristic peaks for rapamycin powder, which confirms the crystallinity of the drug. However, PXRD analysis of rapamycin adsorbed to the surface of PCL films showed the loss of peaks and the presence of a halo pattern between zero and 30 degrees for adsorbed rapamycin, indicating the presence of amorphous rapamycin.

2.4.4 In vivo rapamycin pharmacokinetics

Microporous devices 6 mm in diameter were used for in vivo trials and show constant release kinetics up to 16 weeks (Figure 2.6, Table 2.1). Vitreous concentrations at week 16 were 5.2

ng/mL with a standard deviation of 3.1 (n=5). Retina-choroid concentrations at week 16 were on average 206 ng/g with a standard deviation of 74 (n=5) and were relatively constant over the course of the study. Drug concentrations at four and eight week time points in the vitreous averaged 3.6 +/- 1.5 ng/mL (n=4) and in the retina-choroid averaged 407 +/- 387 ng/g (n=4). The concentration of rapamycin in whole blood and the control eye was below the lower limit of quantitation for the assay (0.5 ng/mL) throughout the study. The outlying data point for vitreous concentration at day 3 may imply a burst release immediately following device implantation before equilibrium is reached throughout the eye. Further in vivo trials may investigate early release behavior of these devices.

Following implantation, eyes were monitored for adverse events and device migration. No evidence of device migration was seen and no evidence of fibrosis or other cellular debris was evident on the devices after explantation (Figure 2.7A). Differences in intraocular pressure (IOP) between pre- and post-implantation eyes were not found to be statistically significant for device and control eyes (Figure 2.7B). The lone adverse event observed was a cataract attributed to surgical trauma during device implantation (Figure 2.7C). No intraocular inflammation was observed during the course of the in vivo study.

2.5 Discussion

The release behavior of rapamycin is dependent upon both device structure and rapamycin crystalline properties. The use of PCL thin films to encapsulate crystalline rapamycin creates a device capable of sustained, zero-order release both in vitro and in vivo. More traditional bulk-loaded films show a characteristic release curve with an initial burst release phase that decays

into a slower rate of release. Microporous PCL devices show a zero-order release curve for rapamycin with a constant amount of drug released per day. Unfeatured rapamycin devices also released drug in a zero-order curve, except with a lower slope owing to the absence of micropores. Due to the small percentage of rapamycin releasing from the devices over the studied period of time, much of the drug mass was still intact. The percentage of drug mass remaining in each in vivo device by week 16 is 84% +/- 15% (Figure 2.8). Future work will further examine the long-term behavior of the devices, including mass balance and release behavior as the devices near exhaustion of their drug payloads.

The zero-order release behavior of unfeatured devices, microporous devices, and un-encapsulated rapamycin pellets was explored by comparing solid crystalline rapamycin to amorphous rapamycin adsorbed onto PCL films. The PXRD results and the in vitro release results support crystallinity as the quality driving slow rapamycin dissolution, which results in linear release rates from these types of encapsulation devices. As the crystal structure of rapamycin is also lost through its dissolution for the formation of rapamycin bulk-loaded films, the release behavior of bulk-loaded films is not dependent on rapamycin crystallinity and instead follows traditional burst release kinetics.⁴⁴

The differences in behavior between rapamycin releasing devices may be attributed to the microporosity of the film, the thickness of the film, and the surface area of crystallized rapamycin available for dissolution. The influence of porosity is seen in the contrast between the release rates of the unfeatured devices when compared to the microporous devices. Drug diffusion through the films is hindered in unfeatured devices due to a lack of pores in their PCL films, while the microporous films have porous networks through their bulk. Varying the thickness of 6 mm unfeatured devices also resulted in differences in cumulative release in the

first 5 weeks, as thicker PCL films decreased the release of rapamycin from the devices.

Modifications to the porous nature, surface area, or thickness of the PCL films are all able to tune the release rate of the loaded drugs to the desired range.

In vivo performance of the microporous 6 mm device demonstrated zero-order release behavior by showing relatively constant vitreous concentrations over time. The concentration of rapamycin in the retina-choroid averaging 206 ± 74 ng/g at 16 weeks demonstrates significantly longer sustained delivery than other rapamycin delivery technologies. A study using repeated injection of solubilized rapamycin in rabbit vitreous in vivo results in a dose-dependent concentration between 109 and 1050 ng/g at four weeks post-injections, followed by a decline to approximately 20 ng/g by eight weeks.³⁰ A study using a nanomicellar eye drop formulation achieved 362 ± 56 (standard error of the mean), but was only measured at 1 hour after a single dose.³⁴ For our in vivo study, there was a large variability in the concentration of rapamycin measured in the retina-choroid for one device measured at week four. For this device the concentration of the drug in the vitreous and the blood did not show a similar increase. Two possible reasons for the increase seen only in the retina-choroid could be the implantation of the device extremely near to the retina, or contamination of the retina-choroid sample during dissection or analysis.

The risk of systemic side effects from this type of device is potentially much lower than other delivery methods. The effective concentration for systemic immunosuppression by rapamycin is typically measured in whole blood at 5-15 ng/mL.³⁰ Concentrations above this range are at risk of side effects. The concentration of rapamycin in whole blood was below the lower limit of quantitation for the assay (0.5 ng/mL) which suggests that local administration of rapamycin in these devices minimizes systemic exposure to the drug and avoids the associated

side effects. Of note, the concentration of rapamycin in retina-choroid is much higher than the 5-15 mg/mL threshold value, which is desirable when targeting the choroid as a site of uveitis. The above-threshold concentrations of rapamycin suggest that an effective dose of the drug exists in the retina-choroid.

The risk of obstructing the visual axis must also be considered, however throughout the course of this study no change in the location of the device was observed. Given the location of the device outside of the visual axis, it is unlikely the device or its soluble degradation products will result in a visual obstruction over the complete lifetime of the device.

An attempt was made with this study to use microvitrectomy to reduce the number of animals required for studying pharmacokinetics in the vitreous. Samples taken from the partial microvitrectomy arm consistently yielded rapamycin concentrations about a factor of 5 lower than samples from the non-microvitrectomy arm. However, samples taken from the animals in the microvitrectomy arm at sacrifice yielded drug concentrations on par with the non-microvitrectomy arm. Thus, for rapamycin it seems that partial microvitrectomy may not yield representative drug concentrations in the vitreous. Potential reasons for this failure may be related to inhomogenous distribution of rapamycin within the vitreous due to altered vitreous structure after repeated partial vitrectomy, the hydrophobic nature of rapamycin limiting diffusion in the vitreous, or the tendency of injected rapamycin to form a drug depot in the vitreous.³⁰ Further work may be necessary to find out if and how this result extends to other drugs administered intravitreally and if the behavior can be predicted by drug hydrophobicity.

The ability to release rapamycin in the vitreous was demonstrated over 16 weeks in vivo, with a drug payload capable of lasting on the order of years, which is significantly longer than

the two months between the necessary dosing of rapamycin by injection.³⁰ Rapamycin concentrations in the vitreous and the retina-choroid were relatively unchanging over the course of the study, demonstrating the potential for a continuous therapeutically effective drug concentration over the lifetime of the drug payload.

2.6 Conclusions

A drug delivery system composed of PCL thin films surrounding rapamycin is an effective means to deliver the drug up to 16 weeks, with the potential for an additional 2-5 years of release. Release behavior of rapamycin is zero-order in both in vitro and in vivo experiments. Drug concentration is high in the retina-choroid site of action after intravitreal implantation, and systemic concentrations are well below the limit for immunosuppression. The release behavior observed in this study may be attributed to the dissolution properties associated with crystalline rapamycin and further research on this property is merited.

2.7 Acknowledgements

We gratefully acknowledge support provided by NIH grant # R01EY021574, and Santen Pharmaceutical Co. We thank San Francisco State University for the use of the Carl Zeiss Ultra 55 FE-SEM and supporting equipment. The FE-SEM and supporting facilities were obtained under NSF-MRI award #0821619 and NSF-EAR award #0949176, respectively. We also thank Research to Prevent Blindness for support of the microsurgery suite used for animal studies, and

UC Office of the President for UC Proof of Concept Grant 247211. We also thank Elliot Chan for his kind assistance.

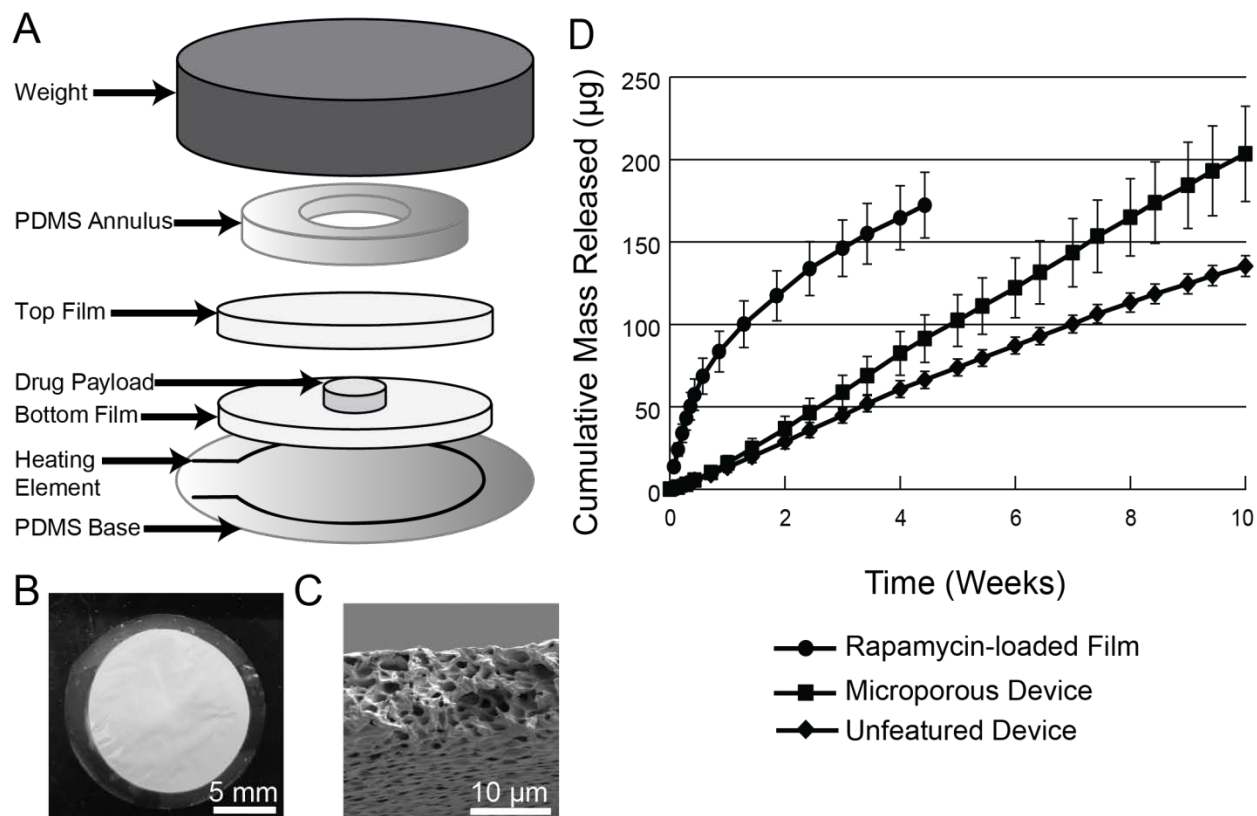


Figure 2.1 Polycaprolactone devices were sealed by heating PCL thin films inside of a weighted jig (a). Loose rapamycin powder was heat-sealed inside of 16 mm microporous devices (b). Microporous PCL thin films were approximately 10 μm in thickness with micron-sized pores throughout its bulk (c). Rapamycin release behavior from a bulk-loaded film shows non-linear burst release while drug release from 16 mm microporous and 16 mm unfeatured devices maintains linear kinetics (d).

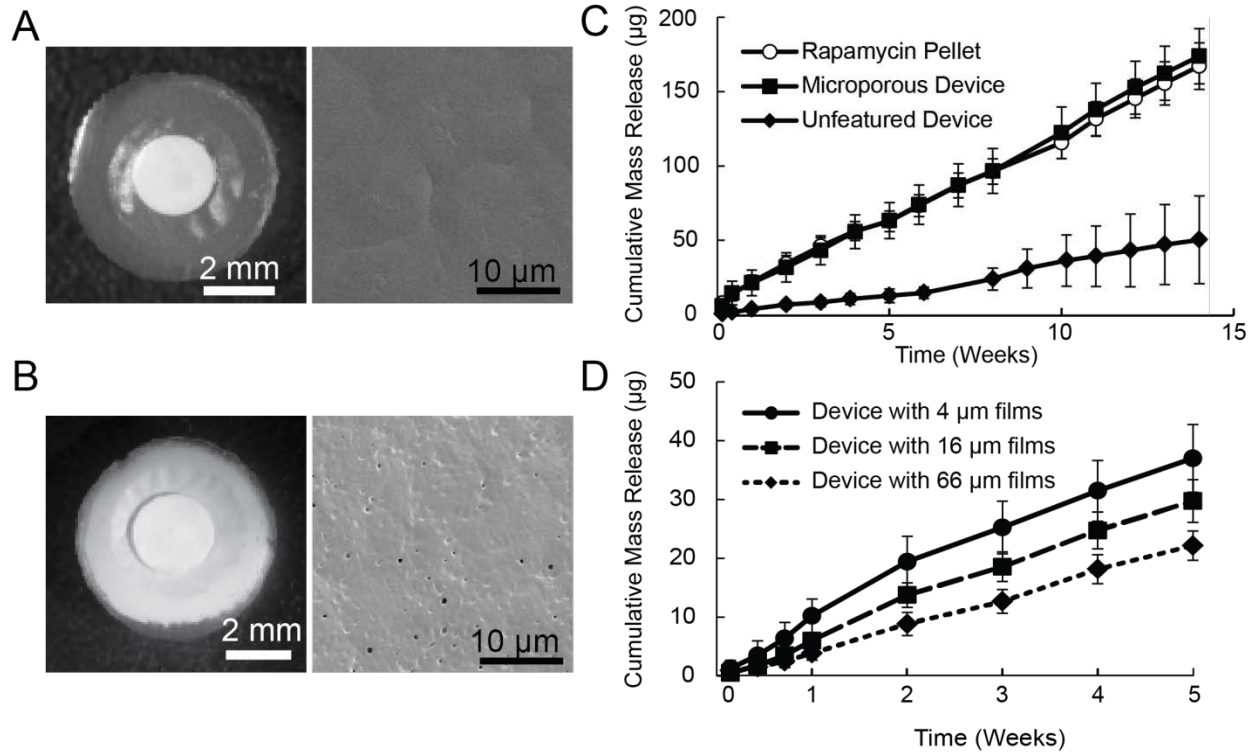


Figure 2.2 Devices 6 mm in diameter and composed of unfeathered PCL (a) or microporous PCL (b). Surface SEMs are also shown for an unfeathered film (a) and a microporous film (b). Rapamycin release from an unfeathered device is significantly lower than release from either a microporous device or a pellet alone (c). Changing the thickness of the PCL films in an unfeathered device results in a correlated change in the release rate of rapamycin (d). For each condition in both (c) and (d), n=4 and error bars are +/- standard deviation.

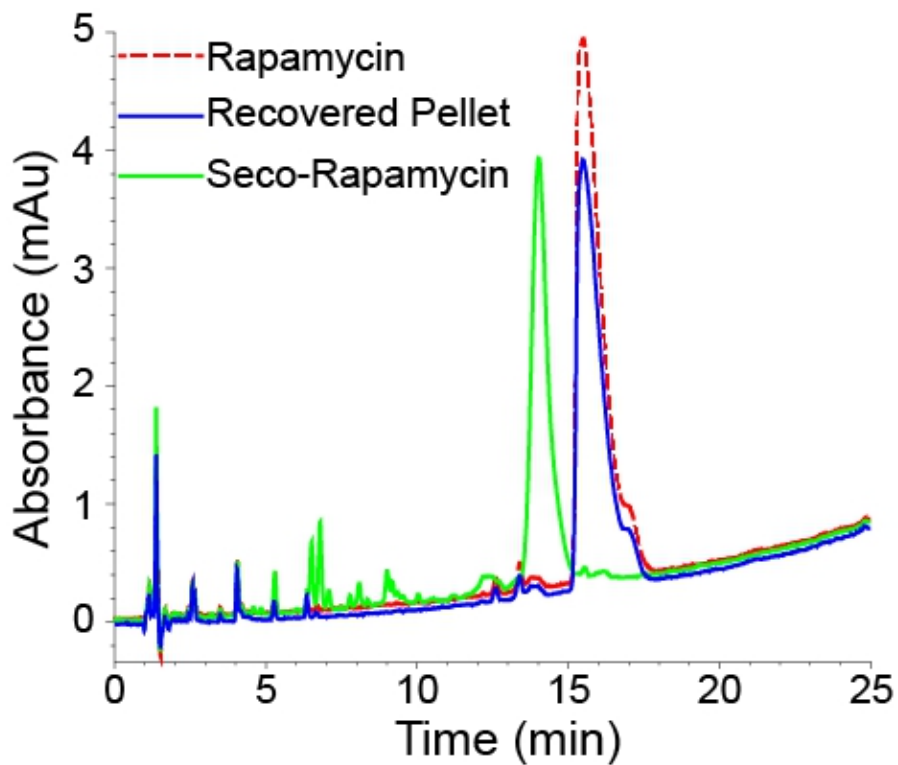


Figure 2.3 An example HPLC trace showing a recovered pellet of rapamycin from a device after 16 weeks of in vitro release (blue line). A positive control of fresh rapamycin (red, dashed line) and seco-rapamycin (green line) are included for comparison.

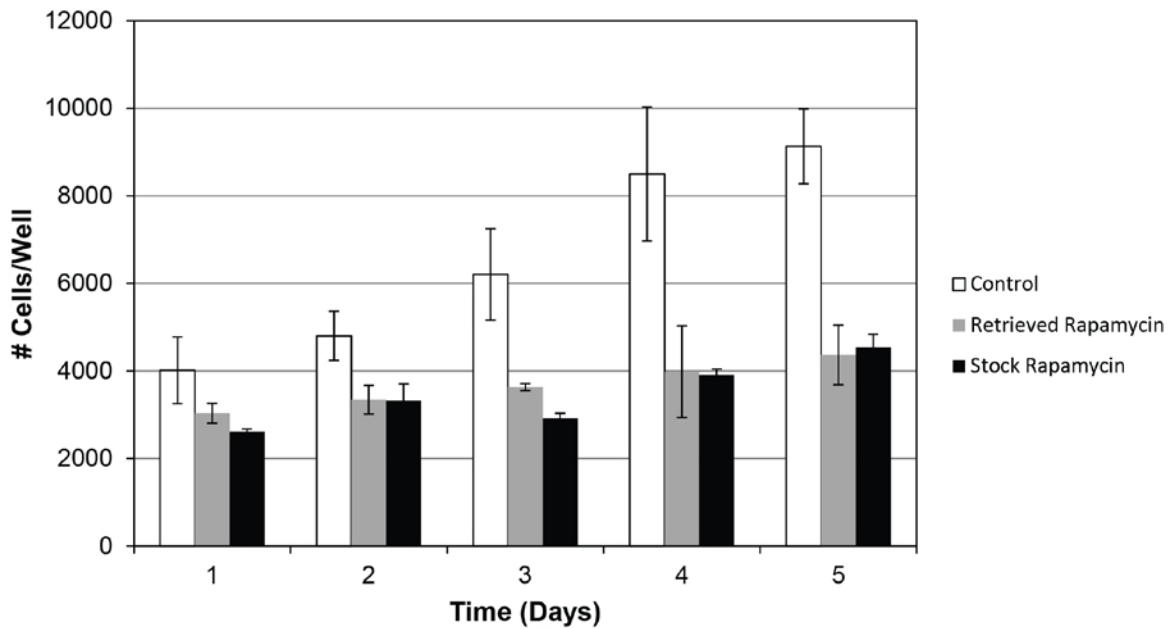


Figure 2.4 In vitro human smooth muscle cell proliferation after exposure to normal media, media with rapamycin retrieved from a drug delivery device after *in vitro* testing, and media with rapamycin made fresh from stock. Rapamycin concentration was 10 ng/mL.

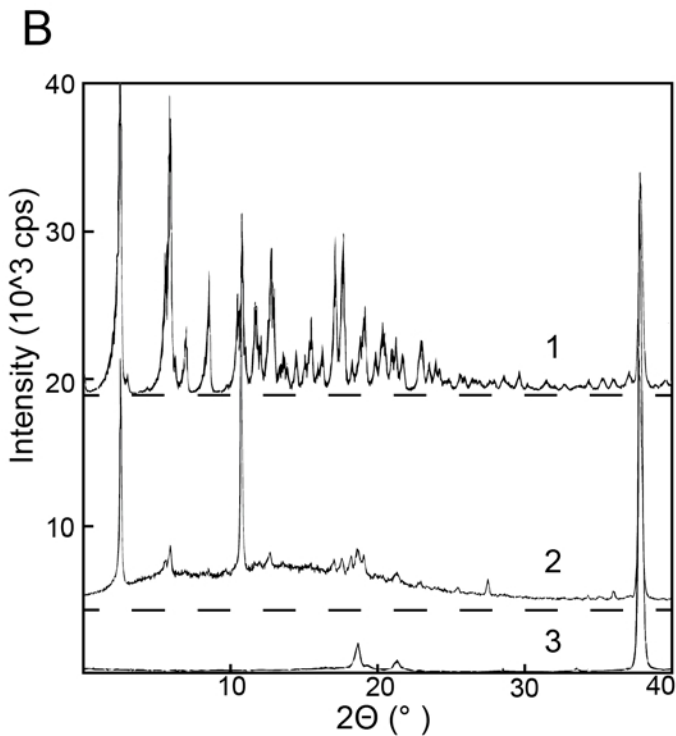
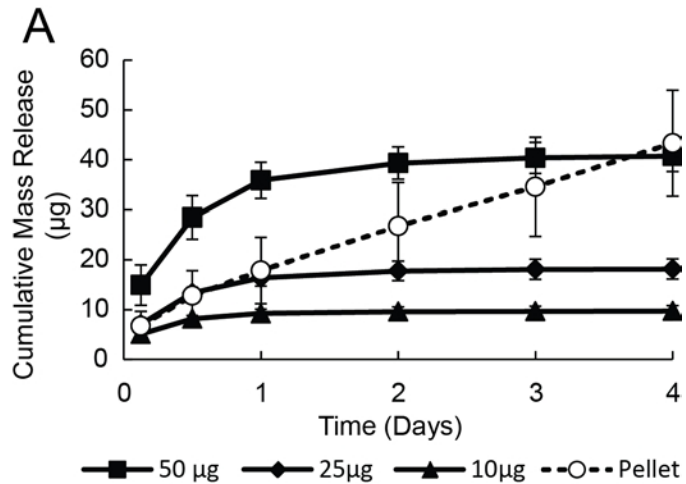


Figure 2.5 Elution experiments (a) of adsorbed rapamycin show non-linear burst release, while rapamycin pellets maintain linear release. Mass given in the legend is mass attempted to adsorb onto the film. For each condition, $n=4$ and error bars are \pm standard deviation. PXRD analysis (b) of rapamycin (1), rapamycin adsorbed onto PCL films (2), and blank PCL films (3). Rapamycin adsorbed onto PCL films (2) shows the gentle hill of a halo effect between zero and

30 degrees for adsorbed rapamycin. The presence of the halo and sharp peaks for adsorbed rapamycin indicates the presence of amorphous and crystalline rapamycin.

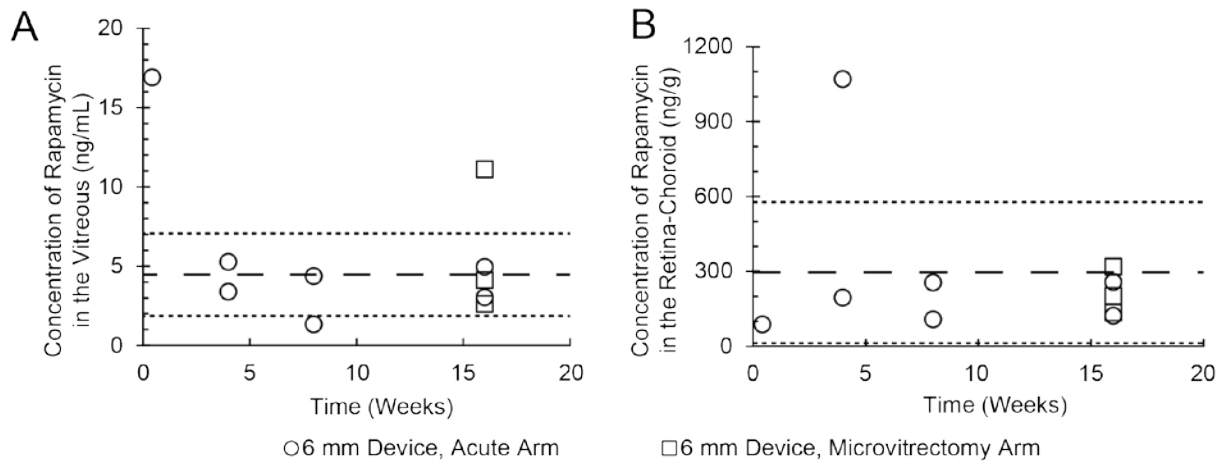


Figure 2.6 In vivo rapamycin release maintained constant rapamycin concentration through 16 weeks as detected in the vitreous (a) and in the retina-choroid (b). Average of the data from weeks 4 to 16 is shown as a dashed line. Average plus or minus the standard deviation is shown as a dotted line. Despite the failings of microvitrectomy as a sampling method (squares), sampling of microvitrectomy-arm animals at sacrifice yielded results consistent with the acute sampling-only arm (circles).

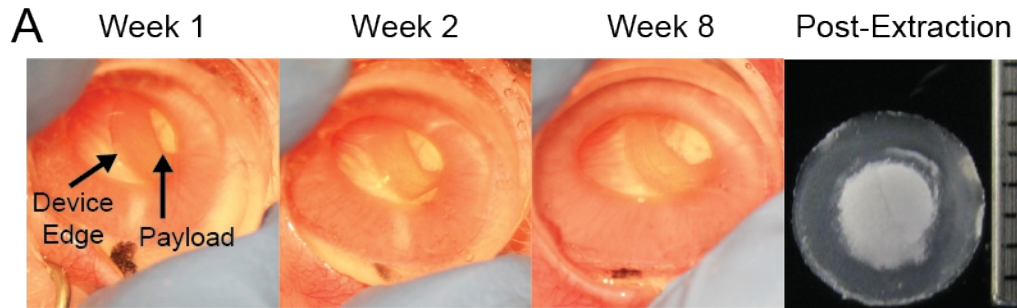
Concentration of Rapamycin in the Vitreous (ng/mL)

Time (Weeks)	0.4	4	4	8	8	16	16	16
6 mm Device, Acute Arm	16.9	3.39	5.27	1.34	4.37	3.04	4.96	-
6 mm Device, Microvitrectomy Arm	-	-	-	-	-	4.11	11.1	2.62

Concentration of Rapamycin in the Retina-Choroid (ng/g)

Time (Weeks)	0.4	4	4	8	8	16	16	16
6 mm Device, Acute Arm	87.8	194	1070	255	107	257	122	-
6 mm Device, Microvitrectomy Arm	-	-	-	-	-	201	134	318

Table 2.1 Values for in vivo concentrations of rapamycin in the vitreous and the retina-choroid.



B

IOP (mm Hg)

	Pre- Implantation	Post- Implantation
Device Eye	13.2 +/- 2.3	16.2 +/- 5.7
Control Eye	14.1 +/- 2.2	17.3 +/- 5.3

C

Adverse Events

	Cataract	Retinal Damage	Conjunctival/ Scleral Damage
Device Eye	1	0	0
Control Eye	0	0	0

Figure 2.7 Devices maintained consistent position in the eye over the course of observation and no fibrosis was found after device removal (a). No statistically significant difference in intraocular pressure (IOP) was found between pre- and post-implantation eyes (b). Only one adverse event was observed and it was attributed to contact between the lens and the device during implantation (c).

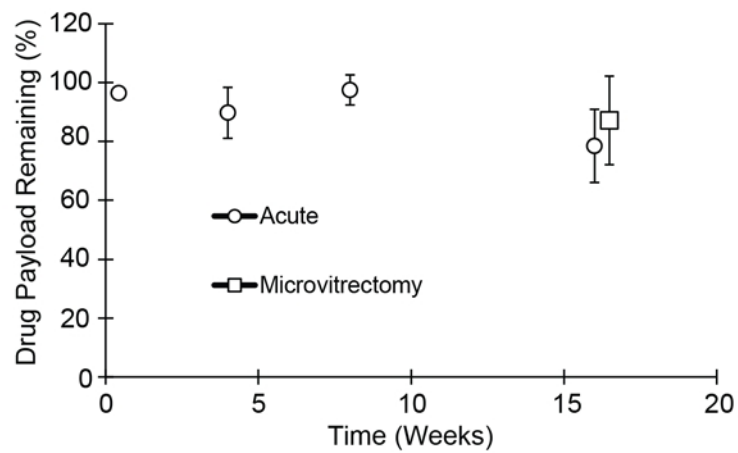


Figure 2.8 Residual drug payloads for in vivo samples as a percentage of their loaded mass.

Week 16 data has been separated laterally for clarity.

Chapter 3 - In Vivo and In Vitro Sustained Release of Ranibizumab from a Nanoporous Thin Film Device

3.1 Abstract

Current administration of ranibizumab and other therapeutic macromolecules to the back of the eye (BOTE) is invasive, costly, and places a high patient load on physicians. Here we introduce a device that produces sustained release of ranibizumab in the BOTE over the course of several months. Our device is composed of twin nanoporous polymer thin films surrounding a ranibizumab reservoir. These devices sustain the release of ranibizumab over 16 weeks in vitro and 12 weeks in vivo, without exhausting the initial drug payload of the devices. Following implantation in vivo, devices were well tolerated and showed no sign of immune response. Our device platform presents a potential solution to the challenge of delivering protein therapeutics to the BOTE for sustained periods of time.

3.2 Introduction

In contemporary ophthalmology, the primary routes of drug delivery are topical drops and intraocular injections. Topical administrations have sustained prominence due to their simplicity and minimal invasiveness. Unfortunately, compliance and persistence are known issues with this route of administration, and clinically proven therapies lose efficacy in real world patient populations.^{45,46} Furthermore, treating BOTE diseases with topical drops is rare given that the permeability of therapeutics is typically insufficient to achieve a therapeutic concentration at the targeted site.⁴⁷⁻⁴⁹ With the introduction of ranibizumab to treat age-related macular degeneration (AMD), intraocular injection became a widespread technique for administration of therapeutic proteins for retinal disease. Following first-in-class ranibizumab, the off-label use of bevacizumab and the approval of aflibercept have diversified the landscape of AMD therapies, as

well as the extension of ranibizumab to treat macular edema.⁵⁰⁻⁵³ With chronic diseases, such as AMD, repeated injections increase the long-term likelihood of an injection-induced trauma or reaction.⁵⁴ In addition, the increased patient load places a notable strain on clinicians that may become unsustainable with current treatment regimens.^{55,56} So despite the effectiveness of intraocular injection, its invasiveness, cost of therapy, and impact on clinicians has led to an as-needed administration mentality for intravitreal therapeutics, which has been shown to decrease their effectiveness.¹⁵ As a consequence, these challenges have spurred substantial development over the past decade to improve BOTE therapeutic delivery.⁵⁷⁻⁵⁹

Currently, injectable ocular devices are capable of sustained delivery of only small molecule therapeutics over the course of several months. Iluvien™ employs a non-degradable device that is capable of achieving relatively constant release rates that gradually slow as the drug payload is expended.⁶⁰ Release can be achieved for up to 3 years, but the carrier material remains resident in the eye after the payload is released. Ozurdex® was a further device iteration that utilized degradable poly(lactic-co-glycolic acid) (PLGA) to avoid accumulation of devices in the eye upon repeated administration.^{61,62} Iluvien® and Ozurdex® are both free-floating implants that may migrate in some patients, but techniques exist to reposition a lost device and generally complications associated with this were minimal.⁶³⁻⁶⁵ Such injectable devices have made major steps to reduce the invasiveness of intraocular delivery, but these technologies were developed around delivery of small molecules and have lacked extension to biologic, large molecule therapies. Consequently, a host of devices seek to address this underserved area.^{57,58,66}

Particle-based drug carriers remain a popular approach to improve therapies because of their capacity to be injected, and unique strategies have been utilized to accommodate biologics.^{67,68} Biosilicon particles are being commercialized for delivery of bevacizumab to the

eye.⁶⁹ Therapeutic is adsorbed onto the particles, and drug release and particle degradation can be modulated based on the surface coating employed. While zero-order release has been achieved with these materials, long duration delivery has not been fully vetted. Alternatively, hydrogel particles formed using the proprietary “particle replication in non-wetting templates” (PRINT) process are being developed for delivery of bevacizumab. Release from hydrogel PRINT particles has been demonstrated through 60 days,⁷⁰ which provides an improvement relative to contemporary ranibizumab injections. In both cases, particles may migrate within the eye, and in the case of an adverse event, repositioning devices or removing them may prove to be impractical given their small distributed nature.

Utilizing a depot approach, ForSight Vision4 is developing a port delivery system (PDS) that employs a reservoir with a subconjunctival port to refill the device with large molecule therapeutic as needed. The PDS device is inserted through the sclera at the pars plana, so device migration is not a concern. The external refill port is positioned under the conjunctiva, accessible for refill injections at intervals, performed in the clinic. A preliminary study enrolled 20 patients and demonstrated good efficacy through 12 months, yet a number of adverse effects were observed, including endophthalmitis, vitreous hemorrhage, and traumatic cataract.⁷¹

Among the technologies being developed for BOTE delivery of large molecule therapeutics, there is an unmet need for an injectable and degradable device capable of long term release. Nanostructured membranes are one method capable of constant-rate release profiles *in vitro* and can achieve sustained release over the course of several months.^{3,2} In these membranes, the membrane pore size is comparable to the molecule size and allows constant-rate release. The nanostructured membrane fabrication processes were designed for compatibility with a variety of polymers, but the degradation properties of poly(caprolactone) (PCL) have made it a preferred

polymer. PCL is a biodegradable polymer that has the property of maintaining physical structure throughout the majority of its degradation: this enables nanostructure-controlled release rates to last for the duration of the drug payload. In addition, nanostructured PCL films have shown excellent biocompatibility in the eye, and their flexibility as thin films may allow them to be furled in an injection device, making this a compelling material for ocular devices.^{4,39}

In this report, a nanostructured biodegradable thin-film device was employed for sustained delivery of ranibizumab to the BOTE. Devices were evaluated for sustained ranibizumab release *in vitro* for 16 weeks and *in vivo* for 12 weeks. To allow accurate measurement *in vitro* and *in vivo*, ranibizumab was fluorescently tagged with fluorescein. *In vitro* release gave an average initial release rate of 1.82 $\mu\text{g}/\text{d}$ and an average terminal release rate of 0.56 $\mu\text{g}/\text{d}$. To account for device-to-device variation, individual device performance was characterized *in vitro* prior to introduction into a New Zealand White rabbit model, where vitreous levels were measured through 12 weeks. Ranibizumab concentrations of 0.83 $\mu\text{g}/\text{ml}$ were attained at 12 weeks, and no adverse effects were associated with device residence outside of implantation trauma. Scanning electron microscopy and quartz-crystal microbalance were both utilized to investigate protein adsorption onto device surfaces, which was shown to be minute. This demonstrates the potential to encapsulate and release protein therapeutics from such devices over sustained durations.

3.3 Materials and Methods

3.3.1 Materials

Polycaprolactone (80 kDa, Mn), 2,2,2-trifluoroethanol (TFE), potassium phosphate monobasic and dibasic, and polysorbate 20 were obtained from Sigma-Aldrich (St. Louis, MO).

Polydimethylsiloxane (PDMS), sodium carbonate, sodium bicarbonate, and L-histidine were obtained from Thermo Fisher Scientific (Waltham, MA). D-(+)-trehalose was obtained from VWR International, Inc. (Radnor, PA). Ranibizumab (Lucentis®, Genentech, South San Francisco, CA) was obtained from the UCSF Department of Ophthalmology.

3.3.2 FITC-Ranibizumab Preparation

FITC-ranibizumab was prepared with a FluoroTag fluorescein isothiocyanate (FITC) Conjugation Kit (Sigma-Aldrich). Briefly, ranibizumab was dialyzed (Slide-A-Lyzer Dialysis Cassette, 10,000 MWCO, Life Technologies, Waltham, MA) in a 0.1 M carbonate buffer (pH 9) and subsequently reacted with the FluoroTag FITC conjugation kit. The product was dialyzed again in a formulation buffer of 10 mM histidine HCl, 292 mM trehalose, 0.01% polysorbate 20, at pH 5.5) and then lyophilized with an AdVantage 2.0 BenchTop Freeze Dryer / Lyophilizer (SP Scientific, Warminster, PA). The resulting formulation used in this study was 6.8% (w/w) ranibizumab. All results reflect the mass of pure ranibizumab, not the mass of the total formulation.

3.3.3 Device Fabrication

Thin films of nanoporous PCL were fabricated as described previously.³ In brief, zinc oxide nanowires were used as a template to define nanopores in a thin layer of PCL that is supported

by a thicker microporous layer. Devices were fabricated by sealing the perimeter of two circular PCL films around a pellet of FITC-ranibizumab (Figure 3.1A). A poly(dimethylsiloxane) (Sylgard, 184, Dow Corning, NY) slab was used as a base support, and heat and pressure were applied by a hollow cylinder of heated metal to fuse the two nanoporous PCL films together. Ice-cold water was introduced to the center of the metal cylinder to prevent excessive heating of the films.

3.3.4 Scanning Electron Microscopy

Nanoporous thin film and device morphology was examined by scanning electron microscopy (SEM) at the device surface and in cross-section. PCL films and device fragments were cross-sectioned by freeze-fracture in liquid nitrogen. Devices were coated with an 8 nm layer of Au/Pd by a Cressington-HR sputter coater and imaged with a Carl Zeiss Ultra 55 field emission scanning electron microscope using an Everhart-Thornley secondary electron detector.

3.3.5 *In vitro* Elution Experiments

Device performance was evaluated *in vitro* by drug elution in 2 mL PBS (pH 7.4) as elution media. Elution studies were performed at 37°C with continuous shaking on an orbital shaker for 16 weeks. Sampling with complete replacement of media was performed at weekly intervals. Twenty-two devices were used for long-term *in vitro* release studies. FITC-ranibizumab concentration in the elution media was measured by plate fluorometer (Fluorocount, Packard Biosciences (PerkinElmer), Waltham, MA), except where high performance size exclusion

chromatography (HPSEC) was used to assay drug aggregation. Results are reported as plus/minus their standard deviations.

3.3.6 *In vivo* Elution Experiments

Prior to *in vivo* implantation, devices were tested for release and seal integrity through *in vitro* testing for 3-4 weeks. After *in vitro* testing, devices were sterilized in 70% ethanol and implanted in the posterior chamber of the right eye of New Zealand White rabbits. The left eye was left as an untreated control. Devices were implanted through a scleral incision and positioned in the posterior chamber out of the visual axis.

FITC-ranibizumab concentration in the vitreous was assayed at weeks 1, 4, 8, and 12 following euthanasia (n=3 at each time point). One rabbit was euthanized prior to week 6 due to complications from an infection unrelated to the device; IOP, adverse events, and device location information was not collected for that rabbit. At each time point rabbit vitreous was completely sampled and devices were extracted. Vitreous was analyzed for FITC-ranibizumab concentration by size exclusion chromatography (see method below). Vitreous was analyzed for FITC-ranibizumab concentration by size exclusion chromatography (see method below). Intraocular pressure (IOP), device location, and adverse events (cataracts, retinal damage, vitreous or aqueous chamber debris, edema, leakage) were tracked to monitor device safety and tolerability. Results are reported as plus/minus their standard deviations.

3.3.7 Post *in vivo* Elution Experiments and Scanning Electron Microscopy

Following device extraction after *in vivo* release studies, devices were imaged using a dissection microscope to examine protein encapsulation and device integrity. Devices were then returned to *in vitro* elution conditions for 3-4 weeks using the methods described above. Following *post vivo* elution studies, the interior and exterior surfaces of the devices were examined by SEM as described above.

3.3.8 High Performance Size Exclusion Chromatography (HPSEC)

HPSEC was used to measure FITC-ranibizumab concentration for *in vivo* vitreous samples and to assess drug stability in both *in vivo* and *in vitro* devices. The remaining drug payload in each device after elution testing was used for HPSEC since the low concentration of eluted samples prevented HPSEC analysis. In brief, an isocratic buffer of 100 mM potassium phosphate (pH = 6.8) and 100 mM potassium chloride was run on an Agilent Bio SEC-5 (5 μ m, 4.6 x 300 mm) column at 0.4 mL/min for 70 minutes. Sample detection was performed via fluorescence (Ex: 495 nm, Em: 525 nm) and spectrometry (Abs: 220 nm, 280 nm, and 495 nm). *In vitro* and *in vivo* samples were compared to a 10 mg/mL solution of FITC-ranibizumab stored at 37 °C as a control.

3.3.9 Quartz Crystal Microbalance (QCM)

Protein adsorption was measured using a Q-sense E4 instrument with 5 MHz gold Q-sense quartz crystal sensors spun-coated with a non-porous layer of PCL. PBS was flowed over sensors at a rate of 50 μ L/min for 10 minutes at 37 °C to measure frequency baselines. Next, a 0.1

mg/ml ranibizumab solution was flowed over sensors at 50 μ l/min for 30 minutes and 37 °C to measure protein adsorption.

3.4 Results

3.4.1 Device Morphology

A pellet of FITC-ranibizumab was encapsulated between two nanoporous films using heat sealing (Figure 3.1A). The PCL films were approximately 20 μ m thick and highly flexible. Assembled devices were 10 mm in diameter with a 6.5 mm diameter reservoir (Figure 3.1B) and the heat-sealed perimeter maintained device integrity even with the osmotic pressure from drug pellet hydration (Figure 3.1C). SEM examination of the device interior and cross-section shows the nanoporous layer and supporting meshwork of microporous PCL (Figure 3.1D-E). The average ranibizumab payload in *in vitro* devices was 177 μ g (\pm 37 μ g), with an average total formulation payload of 2.61 mg (\pm 0.54 mg). The average ranibizumab payload in *in vivo* devices was 189 μ g (\pm 52 μ g), with an average total device payload of 2.78 mg (\pm 0.77 mg).

3.4.2 *In vitro* FITC-Ranibizumab Release

In vitro release of FITC-ranibizumab was recorded through 16 weeks and resulted in a biphasic release (Figure 3.2A). A linear regression fit of the average normalized cumulative released data from day 1 to week 5 has a rate of 0.98% per day ($y=0.98*x+2.4$, $R^2 = 0.990$), while the linear fit for weeks 10-16 has a rate of 0.27% per day ($y=0.27*x+32.41$, $R^2 = 0.997$). On a monthly basis, these rates are 29% and 8.1% of the initial payload is released per month, respectively. The

average residual payload at 16 weeks was 62.8% (\pm 10.8%) of the original loaded payload. The behavior of FITC-ranibizumab released at each time point shows a burst of release in the initial phase of the first five weeks, with a maximum at day 14 where 17 μg of FITC-ranibizumab was released in one week. This initial phase is followed by a gradually diminishing, second release phase up to week 16 where 2.3 μg of drug was released per week (Figure 3.2B). The average initial release rate was 1.82 $\mu\text{g}/\text{d}$ and decreased to an average terminal release rate of 0.56 $\mu\text{g}/\text{d}$. The maximum and minimum release rates for any one-week period was 2.43 $\mu\text{g}/\text{d}$ and 0.32 $\mu\text{g}/\text{d}$, respectively.

3.4.3 *In vivo* FITC-Ranibizumab Release

FITC-ranibizumab was detectable in the vitreous for all 12 weeks of the *in vivo* study. The highest concentration was at week 1 with an average concentration of 2.5 $\mu\text{g}/\text{mL}$ (\pm 1.3 $\mu\text{g}/\text{mL}$), while the remaining time points demonstrate extended release of FITC-ranibizumab through 12 weeks (Figure 3.3A). At 12 weeks, ranibizumab concentrations were 0.83 $\mu\text{g}/\text{mL}$, while the combined average concentration over weeks 4, 8, and 12 was 0.96 $\mu\text{g}/\text{mL}$. Comparing device elution performance during *in vitro* testing both before and after *in vivo* implantation showed less than a 5% change in the rate of drug release (Figure 3.3B).

Upon extraction *in vivo* devices contained a visible yellow FITC-ranibizumab payload, were able to withstand swelling under osmotic pressure, and remained free of fibrous or cellular encapsulation for the implant duration (Figure 3.3C-E). Examination of device surfaces using SEM revealed an intact internal nanoporous layer (Figure 3.3F-G) and an intact external microporous surface (Figure 3.3H). Some protein and salt crystal accumulation is evident in

Figure 3.3F; however Figure 3.3G shows an absence of large scale protein adsorption. The few fissures observed in the nanostructured film (Figure 3.3G) are an artifact of heating during SEM imaging. The external microporous layer is also free of large scale protein residue (Figure 3.3H).

3.4.4 *In vivo* Safety Profile

Devices were well-tolerated following implantation into the posterior chambers of rabbit eyes (Figure 3.4A). No statistical difference was found for IOP between device eyes (12.0 ± 4.6 mmHg) and unimplanted control eyes (12.1 ± 5.3 mmHg) at sacrifice. Likewise, no statistical difference was found between device eye IOP pre-implantation (12.1 ± 4.7 mmHg) and at sacrifice (12.0 ± 4.6 mmHg). The sole adverse events observed were cataracts in the device eye arm of the drug release study (three vs. zero in the control arm); surgical trauma to the lens during device implantation into the small confines of the rabbit eye were the cause of the iatrogenic cataracts. Device location did not vary significantly between implantation and sacrifice time points. Examination of device appearance *in vivo* shows a yellow, convex FITC-ranibizumab reservoir, a white margin of the sealed PCL perimeter around the reservoir, and an absence of fibrous encapsulation or vitreous debris (Figure 3.4B).

3.4.5 Drug Stability and Protein Adsorption

The relative stability of FITC-ranibizumab compared to controls was found to be 114% ($\pm 14\%$) for *in vitro* samples incubated for 16 weeks and 75.5% ($\pm 27\%$) for *in vivo* samples implanted in the rabbit vitreous between 1 and 12 weeks, including an additional 7 weeks of *in vitro* release

testing (Figure 3.5A). The control solution of FITC-ranibizumab maintained 93% stability for 6 weeks at 37 °C, followed by a decay to 52% stability at week 20 (Figure 3.6) Four *in vivo* devices were excluded in this analysis because there was insufficient FITC-ranibizumab for HPSEC analysis following *in vitro* release testing of the recovered devices.

We evaluated the possibility of ranibizumab adsorption on the surface of PCL membranes as a potential means of sample loss or degradation. We used a QCM (sensitive to approximately 1 ng adsorbate per cm² of substrate) to obtain an estimate of the amount of protein adsorbed on the surface of a PCL thin film. Changes in frequency in QCM correspond to changes in mass adsorbed to a surface. When ranibizumab was flowed over a bare gold surface, ample protein adsorption was observed (Figure 3.5B), whereas when ranibizumab was flowed over a gold substrate coated with a thin layer of PCL, no protein absorption was observed.

3.5 Discussion

The controlled release of ranibizumab from our nanoporous reservoir system represents a possible solution to the problem of sustained delivery of ranibizumab to the BOTE. The elution behavior of our device shows a capability to retain and release a ranibizumab payload on the order of several months. The *in vitro* device performance shows sustained release over 16 weeks while only exhausting 62.8% of its initial payload, suggesting that such devices have a potential elution lifetime of approximately 25 weeks under *in vitro* conditions. *In vivo* elution studies in New Zealand White rabbits show therapeutically relevant concentrations of ranibizumab out to 12 weeks. For a ranibizumab delivery device, one can estimate relevant release rates to sustain therapeutic concentrations of long durations.

In previous studies, the half-life of ranibizumab in New Zealand White has been reported to be 2.9d.⁷² Using a one compartment model and assuming a constant rate of drug release, ocular concentrations can be approximated as:

$$C = C_{ss} * [1 - 2^{(-t/t_{1/2})}]$$

where $t_{1/2}$ is time to reach half steady-state concentration and the steady state concentration can be derived as $C_{ss} = (\text{rate of drug release}) * (t_{1/2}) / (\text{vitreous volume}) * \ln(2)$.

Based on these assumptions, ocular concentrations will be within 95% of steady state concentrations after roughly 12.5 days. While a constant rate of release is an imperfect assumption for these devices, given our estimates for the time to approach steady state we can expect the *in vivo* concentrations measured at weeks 4, 8 and 12 will be representative of relevant long term concentrations. Furthermore, using the average terminal release rate of 0.56 $\mu\text{g/d}$ measured *in vitro*, reported ranibizumab clearance ($t_{1/2} = 2.9\text{d}$), and approximate rabbit vitreous volume ($V_{\text{vit}} = 1.7\text{ml}$),⁷³ a steady-state concentration of 1.38 $\mu\text{g/ml}$ is predicted. Variations between *in vitro* and *in vivo* release rates, saturated mechanisms for clearance of ocular ranibizumab, or imperfect estimates for vitreous volumes may contribute to the deviation between the predicted steady-state concentration and the average measured vitreous concentration of 0.96 $\mu\text{g/ml}$ over weeks 4, 8, and 12.

Maintaining a steady-state concentration of ranibizumab allows our device to supply therapeutically effective concentrations of ranibizumab much longer than injections. The IC_{50} range for ranibizumab against VEGF is 11 to 27 ng/mL .¹³ The pharmacokinetic parameters outlined in previous work in rabbits predict that an intraocular injection of 625 μg ranibizumab

will cross this threshold after approximately 45 days (6.4 weeks).⁷⁴ With our device we demonstrate vitreous concentrations of ranibizumab orders of magnitude higher than the IC₅₀ through 12 weeks. Furthermore, such devices are able to achieve this time course with less than one-third the therapeutic payload of a bolus dose.

At the conclusion of *in vivo* studies, devices were recovered and release characteristics were reevaluated *in vitro*. Elution studies performed with recovered devices demonstrate continued constant-rate release, suggesting devices retain their elution capabilities even after weeks of exposure to rabbit vitreous. Examination of devices after extraction shows that device perimeter seals continue to retain osmotic pressure and there is no visible large-scale fibrous encapsulation by proteins or cells. This is expected given the eye's immune privileged nature and previous work with PCL in the eye demonstrating a lack of an inflammatory response.⁴ High magnification SEMs of the device surfaces reveal a nanoporous surface with a mix of open and obstructed pores, likely blocked by aggregates of ranibizumab formed in the highly concentrated interior of the device. It is possible that protein adsorption to nanopores slows drug release *in vivo* resulting in diminished release over time, but is reversed in the protein-free *in vitro* elution media.

Nanostructured PCL films have a history of biocompatibility when implanted in the vitreous.⁴ Implantation of ranibizumab-loaded devices shows no significant increase in IOP over the 12 weeks of our study, along with no change in device location or signs of implant rejection. However, an increased occurrence of cataracts associated with device implantation can be attributed to the challenge of trauma-free surgical implantation in the small rabbit posterior chamber relative to the size of the device. Because devices were designed for human treatment, the smaller vitreous cavity (1.7 ml vs 4.7-5 ml) and the larger lens (thickness 6.7 mm vs 3.89

mm) of this rabbit model compared to human anatomy are expected to contribute to an increased incidence of iatrogenic cataract formation.^{73,75}

When compared to a free solution of FITC-ranibizumab after 16 weeks, encapsulated FITC-ranibizumab in in vitro devices at the same time point maintains a relative stability greater than 100% as measured by HPSEC. This could be attributed to the difference in the hydrophobicity of their surroundings (PCL device vs. polypropylene tube), or exposure to the air interface for the FITC-ranibizumab solution. By comparison, encapsulated FITC-ranibizumab implanted in vivo had a lower stability relative to the free solution of FITC-ranibizumab at matching time points. It is important to note that our formulation of FITC-ranibizumab has not been optimized for long-term stability in a concentrated device reservoir. Future work will be needed to create an optimized formulation for long-term ranibizumab stability and release.

3.6 Conclusion

We have developed a nanoporous, thin film, biodegradable device capable of eluting ranibizumab over the course of multiple months in the posterior chamber of the eye. The device uses nanoporous PCL films to restrict the diffusion of ranibizumab out of a reservoir and has been shown to elute ranibizumab up to 16 weeks *in vitro*. Implantation of the devices into the posterior chamber shows release of detectable amounts of ranibizumab out to 12 weeks with only partial occlusion of the nanopores and no presence of immune encapsulation. Extension of the presence of ranibizumab in the vitreous over the course of months with our device has the potential to improve compliance, reduce the cost of therapy for AMD treatment, and provide an option for long-term delivery of antibody drugs to the posterior of the eye.

3.7 Acknowledgements

This work was supported by funds from National Institutes of Health (R01-EY021574). We gratefully acknowledge use of the Carl Zeiss Ultra 55 FE-SEM and supporting equipment at SF State. The FE-SEM and supporting facilities were obtained under NSF-MRI award #0821619 and NSF-EAR award #0949176, respectively.

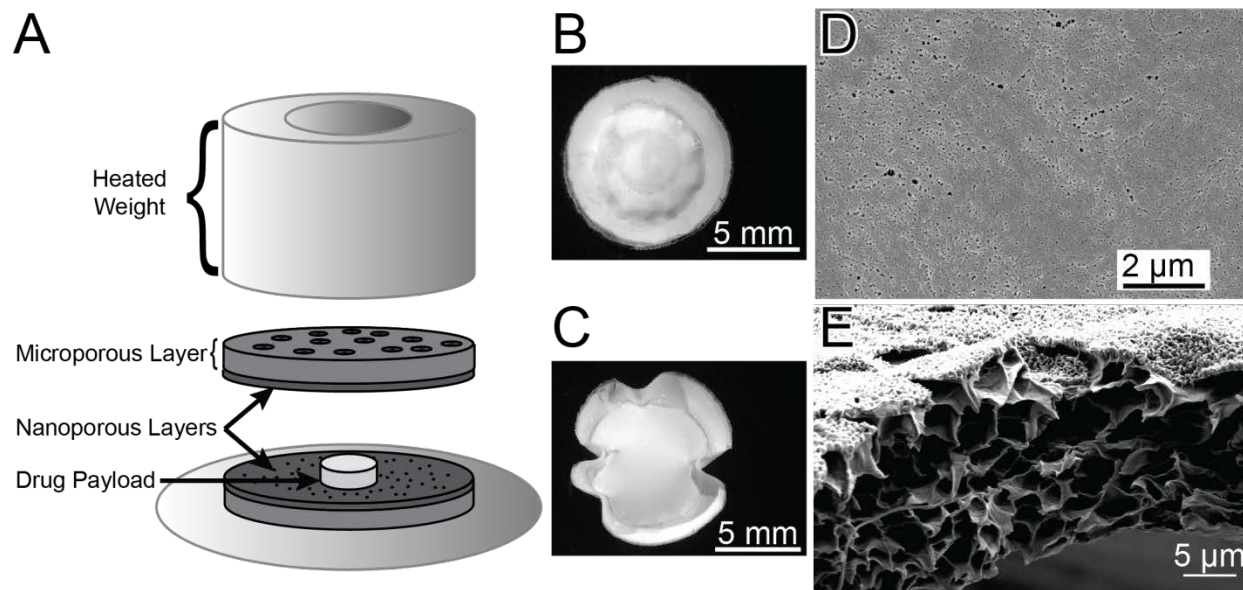


Figure 3.1 Fabrication and morphology of nanoporous devices. (A) Schematic of the sealing process that uses a heated weight to seal two nanoporous films around a drug payload. (dimensions not to scale) (B) Sealed device containing a FITC-ranibizumab pellet. (C) Sealed device after hydration of the drug pellet, where osmotic pressure swells the device's internal reservoir. (D) SEM of the PCL film's nanoporous layer. (E) The nanoporous film in cross-section.

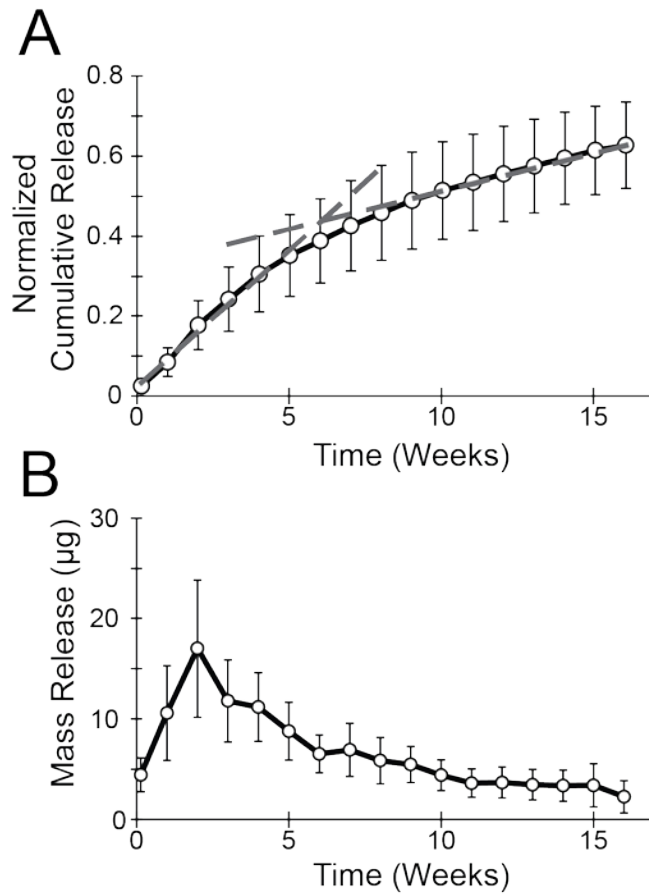


Figure 3.2 *In vitro* release behavior of nanoporous devices. (A) Cumulative release of FITC-ranibizumab, normalized to the initial drug payload mass. The linear fit is shown for day 1 to week 5 ($R^2 = 0.990$) and weeks 10-16 ($R^2 = 0.997$). (B) Drug release shown as mass of FITC-ranibizumab released at each individual time point. $n = 17$ devices.

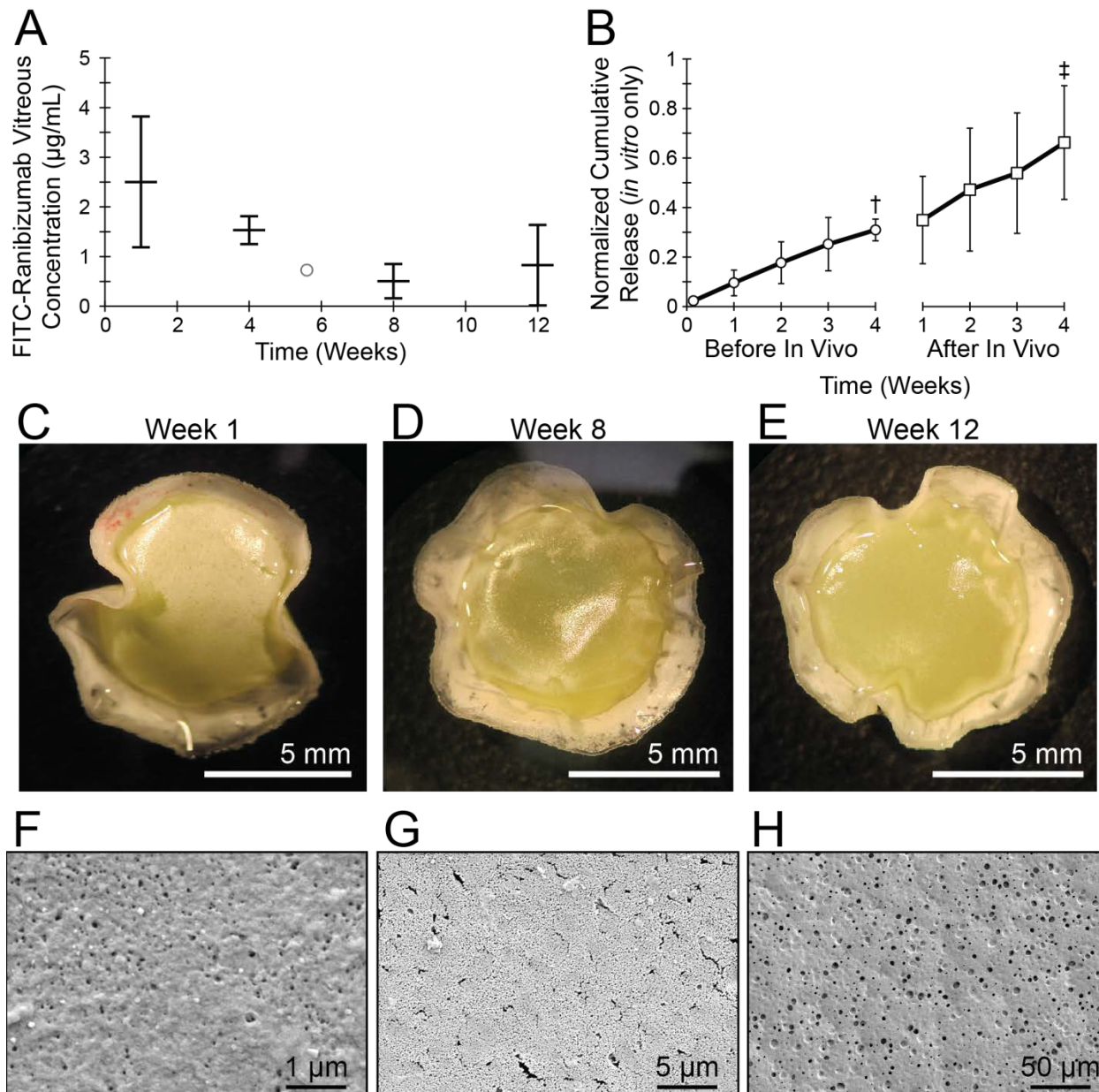


Figure 3.3 *In vivo* behavior of nanoporous devices. (A) Average concentrations of FITC-ranibizumab measured in rabbit vitreous by size exclusion chromatography. The open circle at week 5.6 represents a single measurement. (B) FITC-ranibizumab *in vitro* elution before and after *in vivo* implantation, n=13 devices, except † is n=3 and ‡ is n=10. (C-E) Example devices extracted after (C) 1 week, (D) 8 weeks, and (E) 12 weeks of *in vivo* implantation. (F, G) SEM of the internal nanoporous surface of a device reservoir after *in vivo* implantation. The cracks

visible in (G) are artifacts associated with heating by the scanning electron beam. (H) SEM of the external surface of a device following *in vivo* implantation.

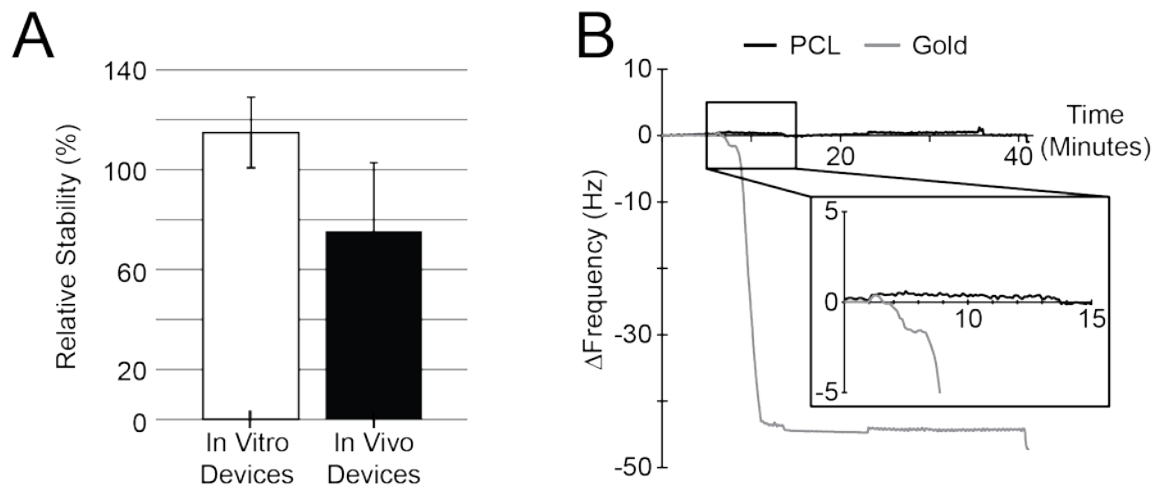


Figure 3.5 Drug stability and adsorption. (A) Stability of FITC-ranibizumab in both *in vitro* and *in vivo* devices normalized to FITC-ranibizumab degradation when not encapsulated in a device. (B) QCM change in frequency for either a gold substrate or a PCL-coated gold substrate following exposure to ranibizumab solution.

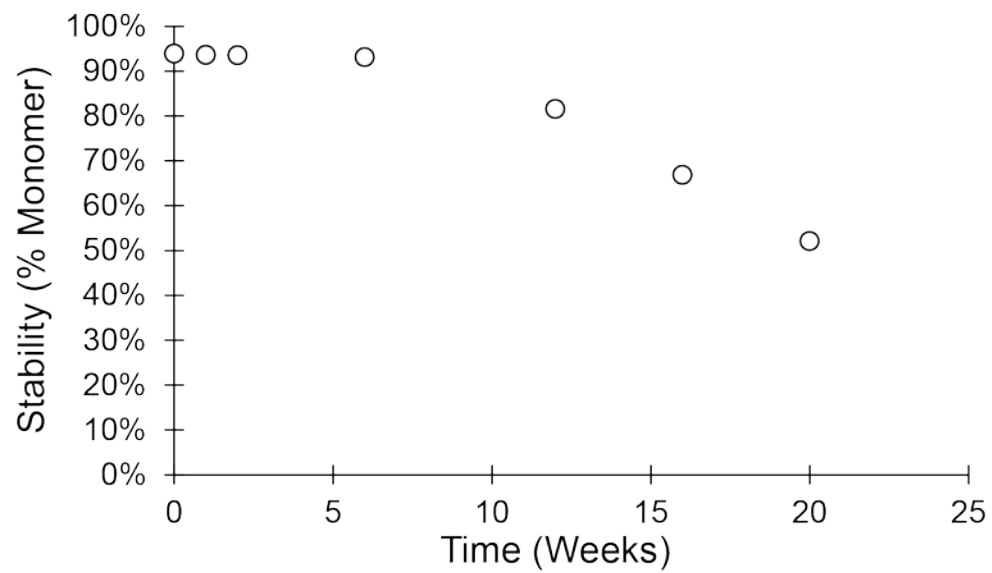


Figure 3.6 HPSEC analysis of FITC-ranibizumab solution stored at 37 °C. Stability is shown as percent monomer relative to total signal.

Chapter 4 - Unidirectional and Sustained Delivery of the Pro-Resolving Lipid Mediator Resolvin D1 from a Biodegradable Thin Film Device

4.1 Abstract

Resolvin D1 (RvD1) belongs to a family of endogenously derived pro-resolving lipid mediators that have been shown to attenuate inflammation, activate pro-resolution signaling and promote homeostasis and recovery from tissue injury. In this study we present a poly(lactic-co-glycolic acid) (PLGA) based thin-film device, composed of layers of varying ratios of lactic and glycolic acid that allows for unidirectional elution of RvD1 to target tissues. The device demonstrated sustained release *in vitro* up to 35 days with a strong linearity up to 14 days. The asymmetric design of the device allowed 98% of the RvD1 released to pass through the layer with the lowest molar ratio of lactic acid to glycolic acid. We validated structural integrity of RvD1 released from the device by mass spectrometry and investigated its bioactivity on human vascular endothelial (EC) and smooth muscle cells (VSMC). RvD1 released from the device attenuated VSMC migration, proliferation and TNF- α induced NF- κ B activation, without evidence of cytotoxicity. Unidirectional RvD1 delivery was demonstrated *ex vivo* in rabbit aortas (in a flow chamber system) and *in vivo* in rat kidney and rat carotid artery. Our results demonstrate a novel approach for sustained, local delivery of Resolvin D1 at therapeutically relevant levels.

4.2 Introduction

Resolvin D1 (7S,8R,17S-trihydroxy-4Z,9E,11E,13Z,15E,19Z-docosahexaenoic acid; RvD1) belongs to a recently discovered class of specialized pro-resolving lipid mediators (SPMs) that promote resolution of inflammation across a wide variety of inflammatory conditions²¹ such as inflammatory bowel disease,⁷⁶ colitis,⁷⁷ sepsis,⁷⁸ endotoxin-induced lung⁷⁹ and kidney injury,⁸⁰ periodontitis⁸¹ and vascular injury.^{22,23} SPMs (lipoxins, resolvins, protectins, and maresins) are

produced endogenously from dietary omega-6 (arachidonic acid) and omega-3 (docosahexaenoic acid and eicosapentaenoic acid) polyunsaturated fatty acids. These SPMs are locally generated from their precursors via trans-cellular biosynthetic pathways involving lipoxygenases in the inflammatory milieu, and are known to down-regulate pro-inflammatory signaling⁸²⁻⁸⁴ through inhibition of NF- κ B activity, attenuation of neutrophil chemotaxis, induction of M1 –M2 macrophage polarization and efferocytosis (clearance of dead cells and leukocytes in the inflammatory zone). Through these actions, SPMs function as homeostatic autacoids, imparting a resolution phenotype within the local environment that has been demonstrated experimentally across a broad range of inflammatory pathologies.^{78,85-88} However, in previous animal studies SPMs were administered through intravenous, intraperitoneal and intra-arterial methods which may be inefficient or impractical for clinical use.^{22,23} Various inflammatory pathologies might benefit from pro-resolving therapeutics, and sustained local delivery of SPMs to target tissues may provide pharmacokinetic benefits, particularly for surgical applications. For example, perivascular delivery of SPMs might improve healing and reduce restenosis after vascular bypass grafting. Likewise, delivery of SPMs to solid organs (e.g. kidney) could be relevant for circumstances of ischemia-reperfusion (e.g. aortic surgery) or after kidney transplantation. We sought to develop a delivery platform for SPM that could be applied in such surgical settings.

An optimal drug delivery device for local perivascular or renal delivery would biodegrade without associated toxicity and release its therapeutic agent at physiologically relevant concentrations selectively to target tissues over a sustained period of time (e.g. weeks). Previous attempts at drug delivery from polymer devices have included wraps, cuffs and hybrid assemblies of PLGA and PCL or both as particles or monoliths, and sometimes are combined with hydrogels. These attempts have aimed to regulate inflammation and proliferation with

various drugs, such as rapamycin,^{89,90} paclitaxel,^{89,91,92} cyclosporine A,⁹³ and sunitinib.⁹⁴

However, clinical use of these agents has been limited due to inherent cytotoxicity associated with their respective mechanisms of action. Furthermore, the unique combination of sustained and unidirectional release of a bioactive lipid compound in a thin film (<100µm) device has not previously been demonstrated.

In the present study, we developed a thin trilayered PLGA device composed of RvD1 loaded between PLGA films of varying ratios of lactic and glycolic acid. This device exhibited controlled release of RvD1 directionally with a 98% bias towards the intended side for drug release. Our device is able to deliver significant levels of stable RvD1 into both vascular tissues and solid organs. The thin and pliable nature of our device facilitates favorable surgical handling, and its biodegradable materials allow for therapeutic applications across a broad range of inflammatory/tissue injury scenarios where sustained, local availability of RvD1 could restore homeostasis.

4.3 Material and Methods

4.3.1 Materials

Polcaprolactone (80 kDa Mn), and 2,2,2-trifluoroethanol (TFE) were obtained from Sigma-Aldrich (St. Louis, MO). PLGA composed of random copolymers of 50:50, 75:25 and 85:15 lactic acid:glycolic acid (L:G) ratios and were obtained from PolySciTech (West Lafayette, IN). Phenol red-free, high-glucose DMEM medium was obtained from UCSF Cell Culture Facility. Polydimethylsiloxane (PDMS) was obtained from Thermo Fisher Scientific (Waltham, MA), and nichrome wire from Consolidated Electronic Wire and Cable (Franklin Park, IL). 17S-Resolvin

D1 and 17S-Resolvin D1 enzyme immunoassay kits were obtained from Cayman chemicals (Ann Arbor, MI).

4.3.2 Device Fabrication

Polymer thin films were spun-cast onto PDMS from solutions of PLGA in TFE. Rectangular pieces of film were laser cut and assembled into a two- or three-layered device with RvD1 loaded in between the layers from a stock of $100 \mu\text{g ml}^{-1}$ RvD1 in 100% ethanol. In bilayered devices, 200 ng RvD1 was loaded between the two films (8mm x 12mm). In trilayered devices used for *in vitro* bioassay experiments and *in vivo* blood vessel studies (8 mm x 12 mm devices) 100 ng was loaded in between both pairs of films for a total of 200 ng RvD1 loaded per device. Trilayered devices used for *in vivo* solid organ studies in rat kidneys (20 mm x 20 mm devices) were loaded with 500 ng RvD1 in between both pairs of films for a total of 1000 ng RvD1 loaded per device. After drug loading the films were annealed together by either an electrified nichrome wire embedded in a PDMS block (for 8 x 12 mm devices) or on top of a hot-plate (for 20 x 20 mm devices). Bilayered devices were made of i) two identical layers of PLGA with L:G ratios of either 50:50, 75:25 or 85:15 or ii) two non-identical layers of PLGA with L:G ratios of 85:15 on one side and either 75:25 or 50:50 on the other side. The trilayered devices were made of 50:50, 75:50 and 85:15 PLGA where the 75:25 PLGA film was placed in between the 50:50 and 85:15 PLGA films. The morphology of the thin film device after fabrication was investigated by scanning electron microscopy (SEM) at the device surface and cross-section. Cross-sections were obtained by freeze-fracture of devices in liquid nitrogen. Devices to be analyzed were coated with Au/Pd by a Cressington-HR sputter coater and imaged with a Carl

Zeiss Ultra 55 field emission scanning electron microscope using a standard Everhart-Thornley secondary electron detector.

4.3.3 *In vitro* Elution Experiments

Device performance was evaluated *in vitro* in phenol red-free DMEM. Devices were incubated in 300 μ L of media in Eppendorf tubes at 37°C while continuously shaken. At different sampling time-points, media was completely removed and replaced with fresh media. Samples were analyzed by EIA.

4.3.4 *In vitro* Directional Elution Experiments

Directional drug elution was studied by isolating each side of a trilayered device in a diffusion chamber. The diffusion chambers were incubated at 37°C with shaking. At different sampling time-points, media was removed and replaced through the sampling ports of the diffusion chamber using a needle and syringe. RvD1 concentrations were assayed by EIA.

4.3.5 Liquid Chromatography-Tandem Mass Spectrometry

Elution samples from *in vitro* experiments were flash frozen in liquid nitrogen and analyzed by liquid chromatography-tandem mass spectrometry (LC-MS/MS) to evaluate the structural integrity of RvD1 released from the device. One volume of methanol containing internal deuterium-labeled standard (d_5 -RvD2) was added to samples to assess extraction recovery. Solid

phase extraction and LC-MS/MS analysis were carried out essentially as described previously.⁹⁵ Briefly, RvD1 was extracted using C18 solid phase extraction cartridges and an automated extraction system (RapidTrace, Biotage). Following extraction, the methyl formate fractions were placed under a stream of N₂ gas until the solvent evaporated. The samples were then resuspended in methanol:water (50:50) prior to injection. Analysis by LC-MS/MS was conducted using a Poroshell reverse-phase C18 column (100 mm x 4.6 mm x 2.7 μm; Agilent Technologies) equipped high performance liquid chromatography system (HPLC; Shimadzu) coupled to a QTrap 5500 mass spectrometer (AB Sciex). The mobile phase consisted of methanol:water:acetic acid (55:45:0.01 vol/vol/vol) and was ramped to 85:15:0.01 (vol/vol/vol) over 10 min, followed by ramping to 98:2:0.01 (vol/vol/vol) over the next 8 min and held for additional 2 min. The entire sample elution was performed using a constant flow rate of 400 μL min⁻¹ at a constant temperature of 50 °C. The QTrap was operated in negative ionization mode using established scheduled multiple reaction monitoring (MRM) transitions⁹⁶ coupled with information-dependent acquisition (IDA) and enhanced product ion-scanning (EPI). RvD1 was identified using retention time and at least six diagnostic MS/MS ions, as compared with authentic RvD1 standard (Cayman Chemical).

4.3.6 *In vitro* Bioassay Experiments

Human greater saphenous veins discarded at the time of coronary or peripheral bypass grafting operations at The University of California- San Francisco (approved by the Institutional Review Board; UCSF Committee on Human Research- Number: 10-03395; the committee waived the need for informed consent) were used to prepare primary cell cultures of EC and VSMC, as

described previously.⁹⁷ Cells of passage 3-5 were used for all experiments. Vehicle or RvD1-loaded (200ng total) trilayered 8 x 12 mm devices were placed inside media contained in a permeable transwell insert of 0.4um pore diameter (Corning, Tewksbury, MA) and the insert was placed above the cells to deliver RvD1 in the following experiments:

4.3.6.1 NF- κ B Assay (p65 Nuclear Translocation)

VSMCs were grown to 70% confluency in 24-well plates and were exposed to devices placed in transwells for 18 hr followed by addition of TNF- α (10ng ml⁻¹) for 2 hours. Total volume of media used per well was 900ul, with 400ul media placed inside the transwell. At 2 hours post TNF- α addition, transwells were removed and cells were fixed with 4% paraformaldehyde and then washed with warm PBS. Cells were then treated with 0.5% Triton-X and fixed in ice-cold methanol for 10min. The VSMCs were then incubated overnight with anti-p65 antibody in a humidified chamber at 4°C and probed the next day with Alexa-488 secondary antibody and visualized under a fluorescent microscope. Media was also sampled at 2 hours after TNF- α addition and assayed for RvD1 levels.

4.3.6.2 Cell Proliferation Assay

VSMCs (passage 3) were seeded on 6-well plates (day 0) in 0.5% media and were serum starved for three days. On day four, cells were exposed to 10% media to stimulate proliferation. A control group was exposed to 0.5% media. At the time of exposure to 0.5% and 10% media, a transwell with a vehicle- or RvD1-loaded device was placed on top of each well. The media was

refreshed at day 6 and 8 and total cell counts were calculated on day 10 using a Neubauer hemocytometer.

4.3.6.3 Migration Assays

VSMCs were grown to confluency on 24-well plates and then serum starved overnight in 0.5% media. The following day mechanical injury in the form of a scratch was made along the center of the well with a sterile tip and PDGF-BB was added to the wells to stimulate migration, except control wells. Vehicle- or RvD1-loaded devices in permeable transwell inserts were then placed over each well. The migratory response was quantified by calculating the area of scratch injury at time of injury and 24 hours later using Image J software (NIH). For EC migration assays the same procedure was followed, except cells were grown in gelatin-coated wells and M199 EC-media (Hyclone Inc, Logan, UT) with 10% serum was used to stimulate migration following scratch wound.

4.3.6.4 MTT Assay

VSMCs or ECs were grown to confluence on 24-well plates in 10% media and exposed to trilayered PLGA device as described above. Cytotoxicity was quantified at 24 hours using a standard MTT Assay (Sigma, St Louis Missouri).

4.3.7 *Ex vivo* Flow Chamber for Vascular Delivery

To study directional drug release from an adventitial wrap to a blood vessel under conditions of flow and convective forces, we created an ex vivo closed-circuit system with continuous pulsatile flow. Flow-chambers were 3D-printed at the UCSF Center for Advanced Technologies (uPrint SE Plus, Stratasys Inc) and pulsatile flow was provided via an external mechanical pump (Colonial Scientific, Richmond, VA). The circuit was completed by inserting segments of abdominal and thoracic aorta harvested from female New Zealand white rabbits obtained through the UCSF tissue-sharing program. To examine directional delivery, we created a co-axial construct. An “inner” vessel (target) was mounted inside the flow chamber and a trilayered perivascular device (85:15 PLGA / 100ng RvD1 / 75:25 PLGA / 100ng Rvd1 / 50:50 PLGA) was wrapped around the inner vessel with the 50:50 PLGA side facing inwards towards the vessel. A second “outer” vessel was then secured snugly outside of the device and inner vessel, to model the perivascular soft tissues. All side branches of both the inner and outer vessels were ligated to ensure a closed circuit. The flow chamber was filled with serum-free media and the mechanical pump was activated to simulate blood flow at approximately 35-40 ml min⁻¹, based on ex vivo flow-rates previously reported. After 24 hours the “inner” and “outer” vessels were removed and homogenized in ice-cold PBS using a glass dounce homogenizer. Lysates were then centrifuged for 15 minutes at 18000 g to remove debris and the supernatant was further purified by centrifuging for 15 minutes at 14000 g through a 30kD cut-off filtration device (Amicon ultra, Millipore, Billerica, MA) prior to RvD1 analysis by EIA.

4.3.8 *In vivo* Drug Delivery Models

Male Sprague-Dawley rats (400-500 g) were used for *in vivo* experiments under an institutionally approved protocol. To evaluate drug elution to a vascular (arterial) target, rats were anesthetized under isoflurane and the left common carotid artery exposed through a midline neck incision. An 8 mm x 12 mm trilayered PLGA device (85:15 PLGA / 100 ng RvD1 / 75:15 PLGA / 100 ng RvD1 / 50:50 PLGA) was wrapped around the common carotid artery (50:50 PLGA film facing the artery) and secured with interrupted 7-0 prolene sutures. After 1 hour, the device was removed and both the left and right carotid arteries were harvested and immediately frozen in PBS. To evaluate drug elution to a solid organ target, rats were anesthetized under isoflurane and the left kidney was exposed through a midline abdominal incision. Two 20 mm x 20 mm PLGA devices (85:15 PLGA / 500 ng RvD1 / 75:15 PLGA / 500 ng RvD1 / 50:50 PLGA) were placed around the anterior and posterior side of the left kidney (50:50 PLGA film facing the kidney cortex). After 3 hours, the devices were removed and both the left and right kidneys were harvested and immediately frozen in PBS. Carotid and renal tissue lysates were assayed for RvD1 as described above (Section 5.3.7).

4.4 Results

4.4.1 Device Morphology

Bilayered or tri-layered devices (Figure 4.1A) were assembled as described above and their morphology was investigated. As thinner film devices composed of PLGA polymers correlate with increased flexibility (Figure 4.1B and 4.1C) and a decreased mass of acidic degradation products, we developed a device with film thicknesses as low as 5-30 μm for individual films, and up to about 50 μm for trilayered devices (Figure 4.1D). 50:50 PLGA films had an average

thickness of 12 μm (± 0.36 SE), 75:25 PLGA films had average thicknesses of 9.9 μm (± 0.55 SE), and 85:15 PLGA films had an average thickness of 26 μm (± 2.0 SE). The PLGA devices were transparent and pliant after fabrication. During in vitro release experiments, devices showed some degree of breakdown and degradation starting after 2 weeks of incubation in release media and ultimately culminating in device fragmentation after week 8 (Figure 4.2). Analysis of the devices by SEM showed cohesion between the multiple layers of the device without any delamination between layers. In cross-section the devices retained discernible strata corresponding to the original films used to make the device, indicating an absence of mixing of polymers between film layers. Surface analysis by SEM showed no change in PLGA morphology following exposure to ethanol, which was used during device fabrication to load RvD1.

4.4.2 In vitro RvD1 Release from Devices

Bilayered PLGA devices composed of films of varying lactic acid:glycolic acid ratios loaded with 200 ng of RvD1 showed slower drug release as the percentage of lactic acid monomer was increased (Figure 4.1E). Bilayered 50:50 PLGA devices showed the fastest release, with 13 μg and 22 μg released in 3 and 5 days, while bilayered devices with an increased lactic acid:glycolic acid ratio of 60:40 decreased drug release to 7.4 μg and 9.3 μg by the same time-points. Changing the lactic acid:glycolic acid ratio to 75:25 resulted in the slowest observed release from any PLGA bilayered device, with 0.8 μg released by day 3, 2.8 μg released by day 5 and 10.6 μg of drug released by day 14. Drug release from 85:15 PLGA devices was above the lower limit of detection for days 7, 12, and 14 (LLOD: 8 pg ml^{-1}), but cumulative RvD1 release by day 14 did

not exceed 0.1 µg. The slow diffusion of drug through 85:15 PLGA layers was incorporated in the design of trilayered devices as a blocking layer for drug diffusion.

We investigated RvD1 release kinetics with asymmetric bilayered and trilayered devices designed to preferentially release drug to one side of the device. The “outer” side was an 85:15 PLGA layer already shown to block RvD1 diffusion, and the composition of the drug-releasing “inner” side was varied. Bilayered PLGA devices had 75:25 or 50:50 PLGA on the inner side. Bilayered devices of the 85:15 PLGA / 200ng RvD1 / 75:25 PLGA design showed 2.2 µg of RvD1 released by day 3 and 3.7 µg released by day 5 (Figure 4.1F). An enhanced release of RvD1 was observed in bilayered devices of the 85:15 PLGA / 200ng RvD1 / 50:50 PLGA design which showed 3.6 µg of RvD1 released by day 3 and 8.6 µg released by day 5. To further increase and extend RvD1 release, a trilayered device was designed with a blocking layer as reserve payload, a slow-release layer as an initial payload, and a fast-release layer with RvD1 loaded in between (85:15 / 100ng RvD1 / 75:25 / 100ng RvD1 / 50:50 PLGA). The trilayered device demonstrated 7.0 µg of RvD1 released by day 3 and 15 µg released by day 5. The 85:15 PLGA / 200ng RvD1 / 75:25 PLGA design also showed the highest average rate of release of RvD1 for weeks 1 and 2 (Figure 4.1G).

The differences between the amount of RvD1 loaded in the devices and cumulative RvD1 eluted by day 35 vary based upon device composition. The trilayered design released 95% of its cumulative total RvD1 by day 14, while the bilayered devices released 83% (85:15 PLGA / 200ng RvD1 / 50:50 PLGA) and 68% (85:15 / PLGA / 200ng RvD1 / 75:25 PLGA) of their cumulative total RvD1 by day 14. By day 35, the total cumulative release of the 85:15 PLGA / 200ng RvD1 / 50:50 PLGA and 85:15 PLGA / 200ng RvD1 / 75:25 PLGA device designs were

20.4 ng (\pm 4.8 ng) and 15.4 ng (\pm 5.8 ng) respectively. For the trilayered device design, the total cumulative release by day 35 was 34.8 ng (\pm 4.7 ng).

4.4.3 Directional *in vitro* RvD1 Release

Directional release from trilayered devices was investigated in a two-sided diffusion chamber that isolated the media exposed to each side of the devices (Figure 4.3A and 4.3B). Directional release from the trilayered devices showed a statistically significant ($p < 0.05$) difference between the two sides as early as day 1 (Figure 4.3C). Differences in cumulative RvD1 release between directional and non-directional release studies can be attributed to the decrease in device surface area exposed to media in diffusion chambers used for directional studies, as compared to non-directional studies performed in Eppendorf tubes.

4.4.4 Assessment of RvD1 Release and Stability by LC-MS/MS

We assessed the structural integrity of RvD1 loaded and released from the trilayered device by LC-MS/MS. Using multiple reaction monitoring (MRM), authentic RvD1 standard showed a retention time of 11.7 minutes and a distinct peak at this same retention time was observed in the device release media at a 3 hour time-point (Figure 4.4A-B). Full MS/MS spectra of RvD1 released from the device showed diagnostic fragmentation ions consistent with that observed for authentic RvD1 (Figure 4.4C).

4.4.5 *In vitro* Biological Assays with RvD1 Eluting Trilayered Devices

In our *in vitro* cell-based assays, we tested the bioactivity of RvD1 released from trilayered devices. RvD1 (nM dose range) has been shown previously to inhibit VSMC migration, proliferation, NF- κ B activity, and to attenuate inflammatory responses in both smooth muscle and endothelial cells.²³ Bioassays testing these vascular cell responses were chosen to confirm bioactivity of RvD1 released from the thin film devices. RvD1-loaded devices inhibited NF- κ B activity in VSMC with a 36% reduction of nuclear p65 translocation after TNF- α stimulus, as compared to vehicle-loaded devices (Figure 4.5A, Figure 4.6). RvD1 levels at the termination of the experiment (20 hrs of net exposure) were 7.1nM (\pm 2.6 SE). RvD1-loaded devices also produced a robust inhibition in VSMC proliferation by as much as 39% when compared to vehicle-loaded devices (Figure 4.5B). In the VSMC proliferation assay RvD1 levels reached 2.3nM (\pm 0.82 SE) and 1.8nM (\pm 0.95 SE) on day 6 and day 8 of the assay, respectively. Similarly, RvD1-loaded devices attenuated VSMC migration by 22% when compared to the vehicle-loaded devices (Figure 4.5C). We also investigated the response of endothelial cells to RvD1-devices in the scratch injury model and found that exposure of endothelial cells to these devices produced no discernible alterations in the endothelial wound healing response (Figure 4.7), suggestive of retention of endothelial migratory function. Moreover, neither RvD1 nor vehicle-loaded devices showed evidence of vascular cell or endothelial cytotoxicity (Figure 4.8).

4.4.6 *Ex vivo* and *in vivo* Delivery of RvD1

A method (see 4.3.7) for detecting RvD1 in rabbit aortic tissue was first validated by analyzing aortic segments spiked with an RvD1 standard (Figure 4.9). We utilized this method for detection of RvD1 in tissues and investigated unidirectional release of RvD1 from the trilayered

devices *ex vivo* in a closed-loop system with pulsatile flow (Figure 4.10A, Figure 4.11). A segment of rabbit aorta was mounted in the flow system, a device was placed circumferentially around it, and then a second aortic segment was wrapped external to the device in a snug fashion (Figure 4.11). RvD1 levels measured in the outer vessel were found to be $0.094 (\pm 0.016 \text{ SE})$ pg RvD1 per mg artery, versus $0.413 (\pm 0.118 \text{ SE})$ pg RvD1 per mg artery in the inner vessel (Figure 4.10B, $p = 0.03$).

Finally, we validated drug release to various tissues *in vivo* in an acute rodent model. The common carotid artery was used as a prototype vessel and the kidney as a prototype solid organ. We found that application of our trilayered device placed around the left carotid artery (LCA, Figure 4.10C) resulted in significantly higher levels of RvD1 compared to contralateral controls (native right carotid artery, RCA) at one hour post-application (Figure 4.10D). The level of RvD1 in LCA was $0.628 (\pm 0.042 \text{ SE})$ pg RvD1 per mg tissue compared to $0.119 (\pm 0.073 \text{ SE})$ pg RvD1 per mg tissue in RCA. Since kidneys are much larger in size and have much greater tissue mass than blood vessels, we used two 20 x 20 mm devices, each loaded with 1000pg of RvD1, and allowed the two devices to remain for 3 hours after placement. Application of PLGA devices around the left kidney (Figure 4.10E) resulted in significantly higher levels of RvD1 compared to contralateral controls (native right kidney, Figure 4.10F).

4.5 Discussion

PLGA is well documented as a biodegradable polymer with a long history in the field of controlled drug delivery. This paper introduces a device that uses multiple thin film layers of varying compositions of PLGA to release the bioactive lipid mediator RvD1 in a sustained and

unidirectional manner. This approach to drug release allows for simple modulation of drug release kinetics, changes in payload, modifications in size and shape, and the potential for generalization to deliver other small, hydrophobic drug molecules, especially lipid-based drugs or bioactive compounds.

Much of the previous work in the field of drug delivery has involved the use of biodegradable polymers, thin film technologies and directional release, but rarely have all of the three components overlapped. Thin film devices have been used previously to deliver anti-proliferative drugs to the vasculature. One such example involved PLGA and PCL films of 50 μ m thickness created by solvent casting with rapamycin co-dissolved within the polymers.⁹⁰ Although both PLGA and PCL films allowed for sustained release in this study, neither facilitated unidirectional release of rapamycin. Previous work on unidirectional release to tissues has been demonstrated for delivery of sunitinib in combination with PLGA films and hydrogels.⁹⁴ Directionality was achieved by loading sunitinib into hyaluronic acid hydrogels loaded on porous PLGA films laid on top of a non-porous impermeable PLGA. This device allowed for directional release of sunitinib from the hydrogel as non-porous PLGA was impermeable to the drug. However the device is limited by thickness, and had a strong dependency on drug choice and formulation. Another approach towards achieving unidirectional release utilized polymer thin films in an asymmetric layer-by-layer assembly.⁹⁸ In this approach, a thick 85:15 PLGA film formed a blocking layer on one side of the device and a thin 85:15 PLGA film formed a permeable capping layer on the other side of the device. The core of the device was an alternating layer-by-layer assembly of poly(allylamine hydrochloride)–dextran and hyaluronic acid loaded with negatively charged methotrexate held to the polymers by ionic interactions. Unidirectional release in a thin, flexible polymer film was achieved, but release was

over 90% depleted after four days, and drug selection was limited to a strong ionically charged molecule.

While many of the previously studied anti-inflammatory and anti-proliferative agents have been found to possess inherent cytotoxicity, therapeutic delivery of endogenous pro-resolving lipid mediators like RvD1 is attractive for the potential of homeostatic bioactivity without toxicity. Rodent studies using RvD1 and other SPMs have largely been limited to systemic intravenous, intraperitoneal and intraarterial delivery, whereas sustained and local delivery of SPMs has remained relatively unexplored. In a recent study RvD1 was incorporated into chitosan scaffolds by adsorption followed by lyophilization,⁹⁹ and was used locally to favorably modulate the immune response in a mouse model of air-pouch induced inflammation. However, this chitosan construct did not provide sustained release of RvD1. While this study demonstrates relevance of local delivery to harness the pro-resolution activity of RvD1, chitosan scaffolds are a less viable option for therapeutic SPM delivery to tissues or organs as they lack directionality and ability to release RvD1 over an extended period of time. Lastly, humanized nanoparticles incorporating RvD1 or a stable analog of another SPM, lipoxin A₄, showed enhanced bioactivity in murine models of inflammation, further supporting the view that the biological actions of SPM can be enhanced for targeted therapeutic approaches.¹⁰⁰

Our trilayered device is designed with an outer layer to block the diffusion of RvD1 (85:15 PLGA), a middle layer to allow slow diffusion of RvD1 (75:25 PLGA), and an inner layer to allow rapid diffusion of RvD1 (50:50 PLGA). Two separated drug reservoirs allow for independent payloads, one for rapidly releasing drug and the other for slower sustained release. In agreement with these design goals, faster release of RvD1 occurs from the 50:50 PLGA inner side while minimal release is observed from the 85:15 PLGA outer side. Increased water

penetration through films with higher percentages of glycolic acid may assist enhanced diffusion of RvD1 through the membrane. Alternatively, when compared to 85:15 and 75:25 PLGA, 50:50 PLGA is more amorphous and less crystalline which may present a lower barrier to RvD1 diffusion. Future work is needed to determine the mechanisms governing diffusion of RvD1 and other molecules within the same class of pro-resolving lipid mediators.

The incorporation of RvD1 into our device without exposure to the extreme temperatures of melt casting, polymerizing radicals, or reactive solvents allows us to maximize the stability of the loaded drug. *In vitro* quantification by immunologic binding in an EIA and bioactivity in cellular assays validates the elution of bioactive RvD1 from the devices. EIA detection used for *in vivo* experiments further verifies the presence of RvD1 in both blood vessels and solid organ tissues. LC-MS/MS analysis of media collected from trilayered wrap elution experiments revealed the presence of RvD1 that matched the retention time of authentic RvD1. This shows that the fabrication of the trilayered device does not degrade its RvD1 payload and the device is able to elute intact drug. Furthermore, in our RvD1 release studies with carotid artery and kidney models, EIA analysis has confirmed the release of RvD1 from our devices into the target tissue.

RvD1 has been shown to impart protection in the context of arterial injury (restenosis),^{22,23} inflammatory bowel disease,⁷⁷ ischemia/reperfusion⁸⁰ and endotoxin induced acute kidney injury.¹⁰¹ Vascular inflammatory diseases like atherosclerosis and restenosis are associated with endothelial injury and vascular smooth muscle cell proliferation and migration within the vessel wall resulting in intimal hyperplasia. We demonstrate here that RvD1 released from the device promotes an anti-inflammatory phenotype in vascular smooth muscle cells by attenuating their proliferation, migration and NF- κ B activation. We believe this device has therapeutic potential in a variety of inflammatory pathologies, such as after vascular bypass and

solid organ transplantation. The design of the RvD1-releasing device can be modified to fit various situations by altering device dimensions, payload, and polymer composition.

4.6 Conclusions

We have developed a low mass, surgically adaptable, biodegradable and trilayered thin film PLGA device capable of sustained, unidirectional release of the pro-resolving bioactive lipid mediator RvD1. Our device directionally releases RvD1 to the target tissue of interest, and the design can be modified to fit various organs by altering dimensions, shape, payload, and release kinetics. Eluted RvD1 was identified by immunologic detection in an enzyme immunoassay and by LC-MS/MS analysis, and exhibited biological activity on human vascular smooth muscle cells without associated cytotoxicity. These devices were able to deliver therapeutically relevant levels of RvD1 *ex vivo* and *in vivo* to organs and tissues with curved and tubular geometry. Furthermore, the pliable nature of the device allows for direct adherence to blood vessels and solid organs, and is thus applicable to a variety of acute and sub-acute inflammatory pathologies, such as ischemia-reperfusion, endotoxin-induced injury and vascular injury. This biodegradable device holds therapeutic potential for a broad range of surgical interventions where sustained local delivery of pro-resolving lipid mediators may impart beneficial effects.

4.7 Acknowledgements

This work was supported by funds from National Institutes of Health (HL106173; HL119508; HL123318-01A1), Vascular Intervention/Innovation and Therapeutic Advances contract

(HHSN268201400005C). We gratefully acknowledge use of the Carl Zeiss Ultra 55 FE-SEM and supporting equipment at SF State. The FE-SEM and supporting facilities were obtained under NSF-MRI award #0821619 and NSF-EAR award #0949176, respectively.

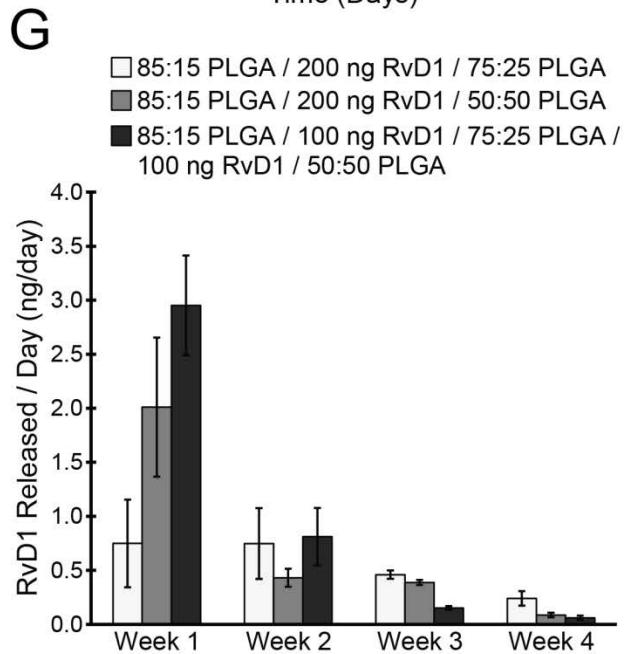
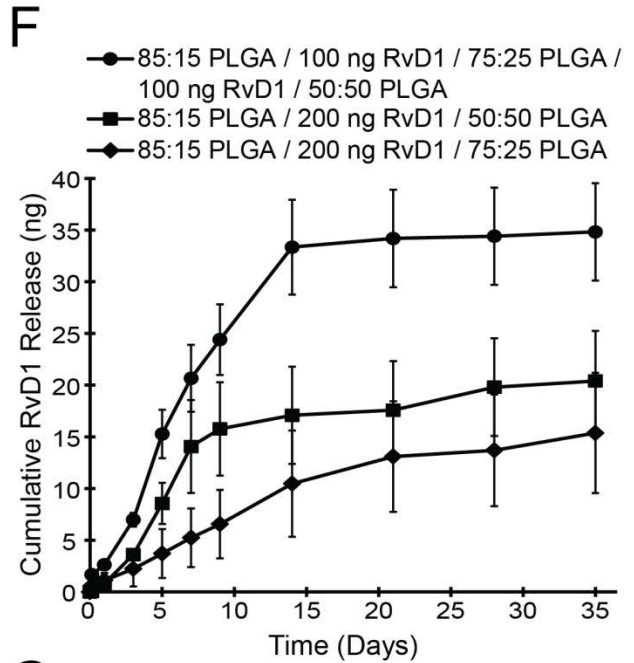
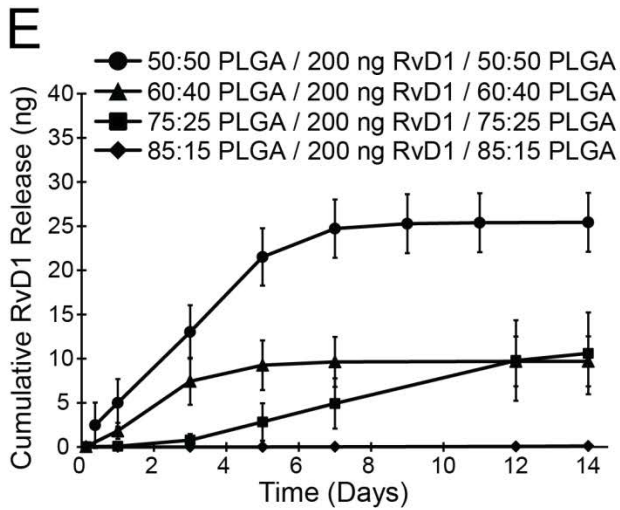
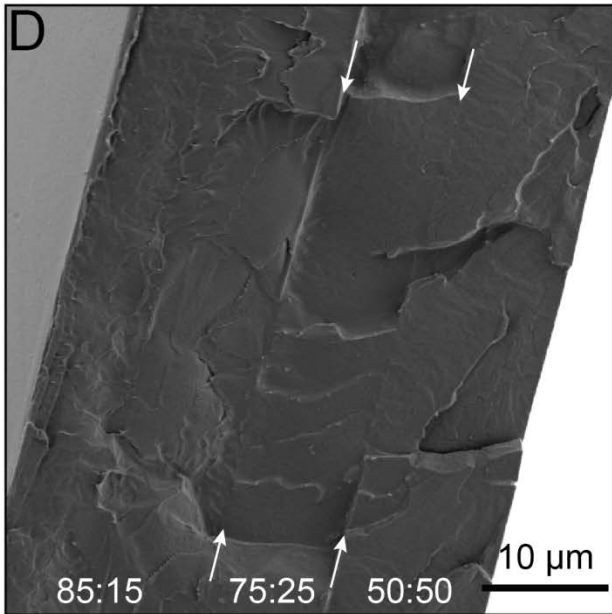
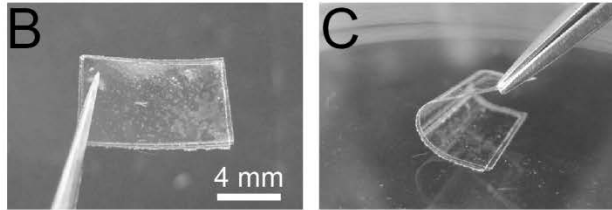
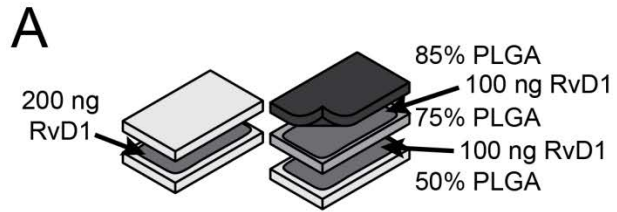


Figure 4.1 Assembly and elution characteristics of PLGA devices. (A) Schematic diagram of assembled bilayered and trilayered devices. (B-C): Picture of the trilayered (85:15 PLGA / 100 ng RvD1 / 75:25 PLGA / 100 ng RvD1 / 50:50 PLGA) device in flat (B) and bent (C) form. (D) Scanning electron micrograph of cross-section of a trilayered device with PLGA ratios of each layer labelled. Arrows indicate film interfaces. (E) Cumulative RvD1 release from bilayered PLGA devices of varying lactic:glycolic acid ratios. (F) Cumulative RvD1 release from PLGA devices of varying lactic:glycolic acid ratios and designs. (G) Average RvD1 released per day for weeks 1 to 4.

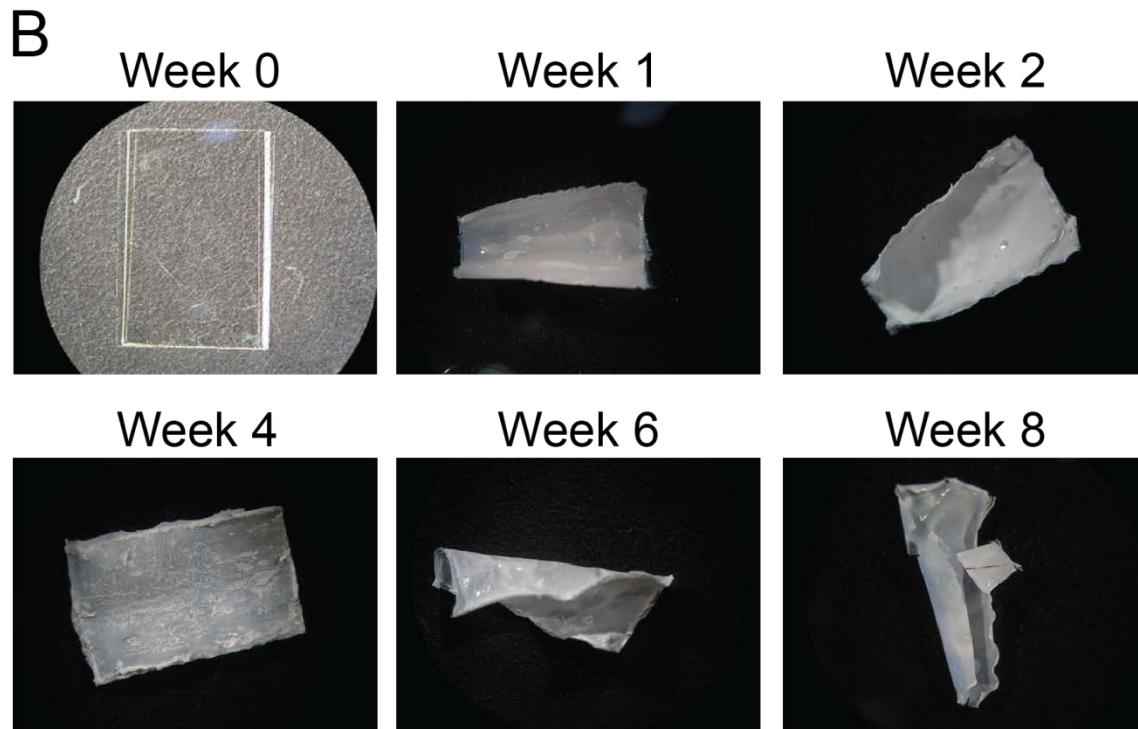
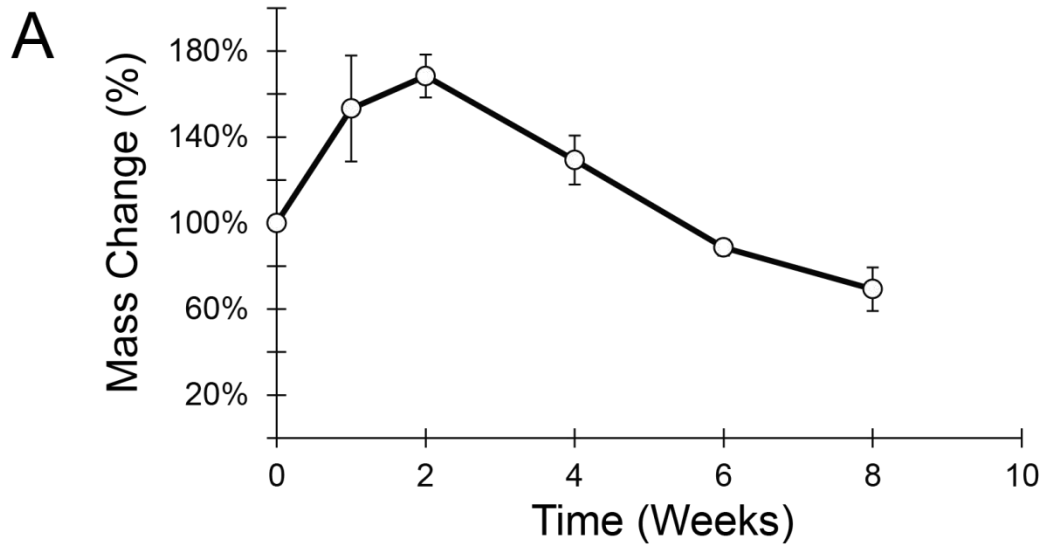


Figure 4.2 Mass change and morphology change of trilayered devices (85:15 PLGA / 100 ng RvD1 / 75:25 PLGA / 100 ng RvD1 / 50:50 PLGA) over time in elution media.

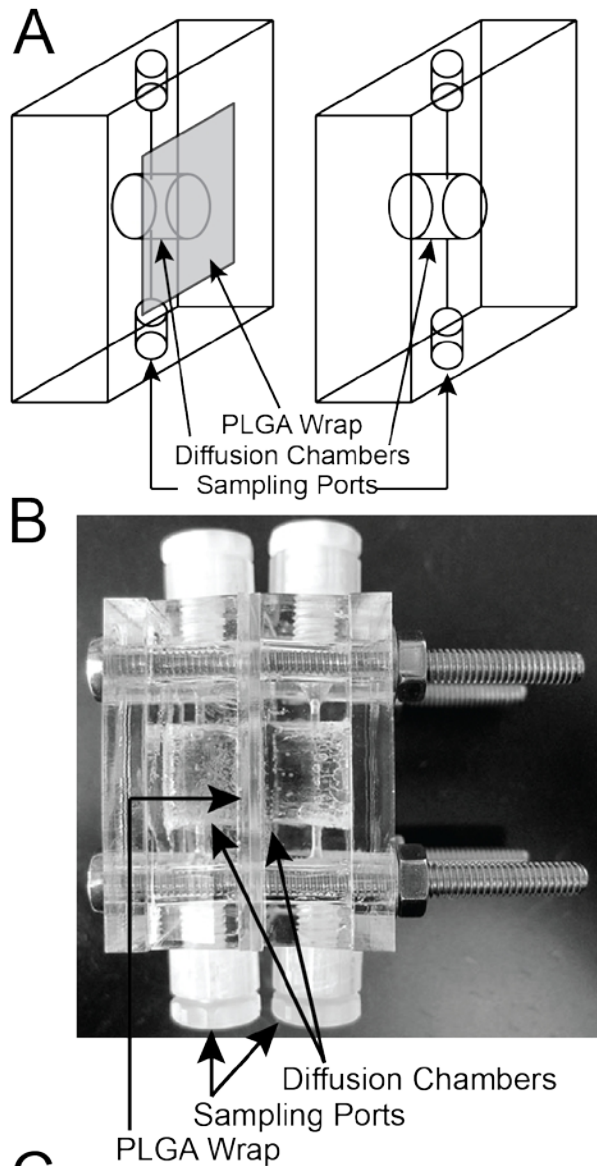
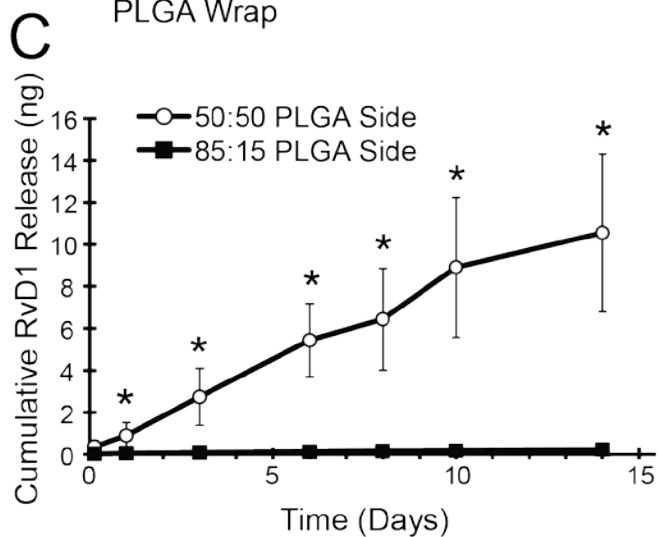


Figure 4.3 Directional release of RvD1 from the trilayered 85:15PLGA / 100ng RvD1 / 75:25 PLGA / 100ng RvD1 / 50:50 PLGA device. (A-B) Schematic representation (A) of the device (B) used to study RvD1 release from two sides of the trilayered PLGA devices. RvD1-loaded PLGA devices were placed in between the two halves of the cube, and diffusion chambers were filled with media, which was sampled from each side and replaced through the side ports at each time-point. (C) Cumulative RvD1 released from each side of the trilayered PLGA construct. * = $p < 0.05$ between sides.



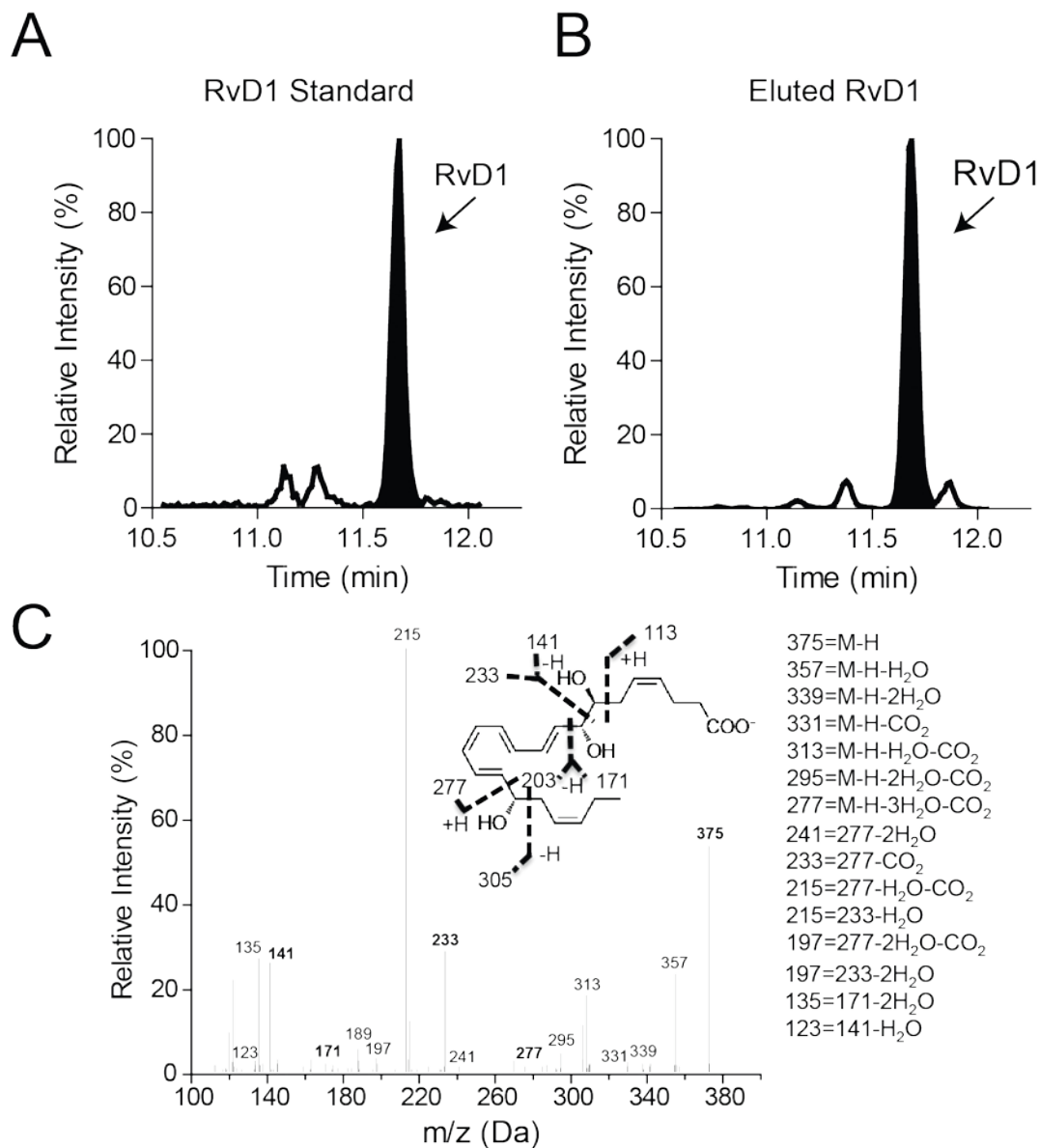


Figure 4.4 Identification and quantification of RvD1 released from trilayered PLGA devices. Representative MRM chromatograms are of (A) RvD1 standard and (B) RvD1 released in the media from a trilayered device. RvD1 released into the media was identified using multiple reaction monitoring (MRM), retention time and diagnostic MS/MS fragmentation ions as compared with authentic RvD1 standard. The retention time matching the RvD1 standard (11.7

min) is shaded in black. (C) Full MS/MS spectra of eluted RvD1 with diagnostic fragmentation ions used for identification indicated as inset.

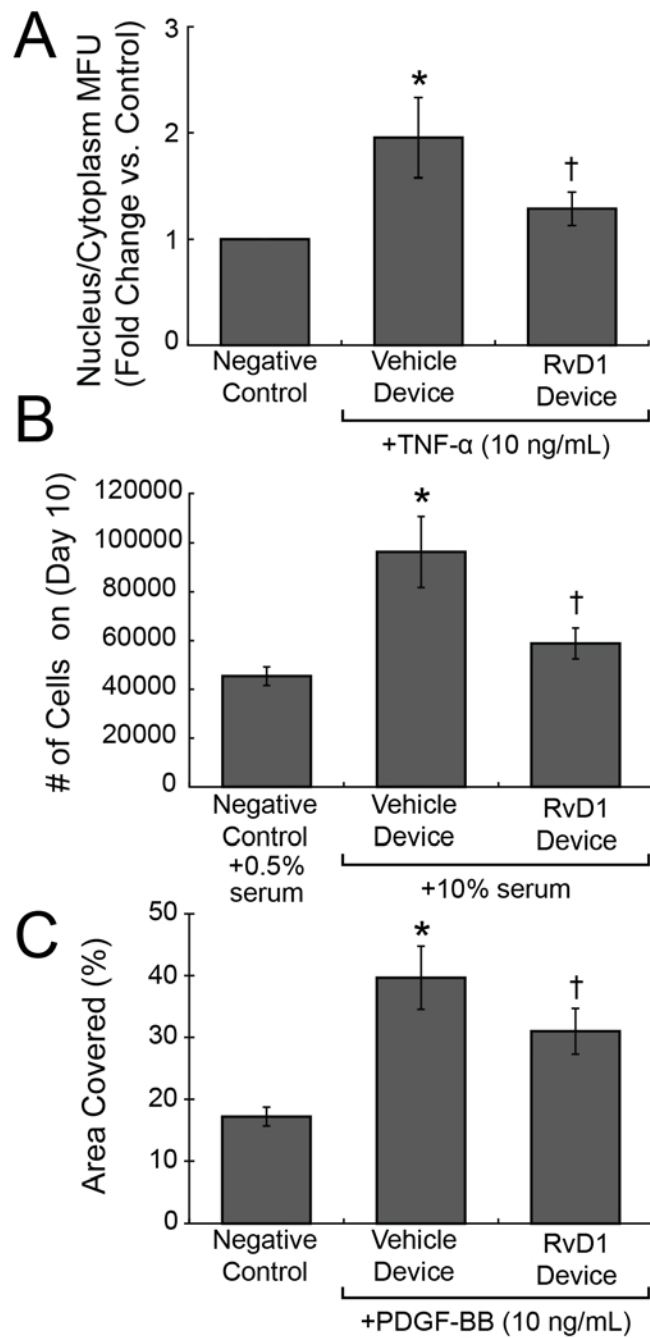


Figure 4.5 Biological activity of RvD1 released from trilayered 85:15 PLGA / 100ng RvD1 / 75:25 PLGA / 100ng RvD1 / 50:50 PLGA device. (A) Human vascular smooth muscle cells were incubated with vehicle- or RvD1-loaded PLGA device in a transwell for 18hr, followed by

vehicle or TNF- α (10ng ml⁻¹) for 2 hours, in the presence of the device. N=3 per group and multiple images were taken from each well at random to quantify net p65 nuclear translocation.

(B) VSMC were seeded in 6 well plates and after 2 days of serum starvation, were exposed to 10% serum containing media (day 0) as a proliferative signal in the presence of vehicle- or RvD1-loaded devices. Cells were counted at day 10. N=3 per group. (C) VSMC was grown to confluency in 24-well plates and the area of migration was quantified at 24 hours following a scratch wound in the presence of PDGF-BB (10 ng ml⁻¹). RvD1-loaded devices inhibited VSMC migration significantly compared to vehicle-wraps. N=4 per group. * = p<0.05 from vehicle device controls; † = p<0.05 from vehicle device exposed to TNF- α , 10% media, or PDGF-BB.

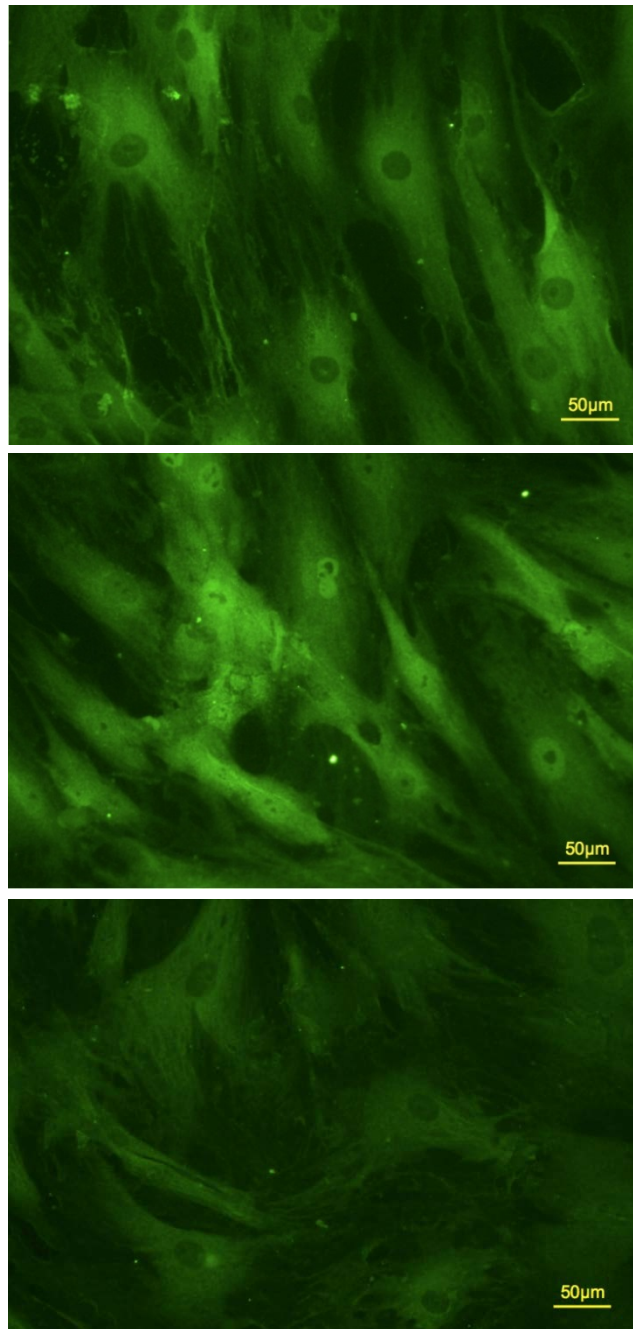


Figure 4.6 Translocation of p65 from exposure to trilayered 85:15 PLGA / 100ng RvD1 / 75:25 PLGA / 100ng RvD1 / 50:50 PLGA device. (A-C) Human vascular smooth muscle cells were incubated with vehicle- or RvD1-loaded PLGA device in a transwell for 18hr, followed by

vehicle or TNF- α (10ng/ml) for 2 hr, in the presence of the wrap. (A) shows minimal p65 nuclear translocation in the presence of vehicle device without any TNF- α . (B) shows p65 translocation in a large subset of cells, which had vehicle device exposed to TNF- α . (C) illustrates robust inhibition of nuclear p65 translocation in the cells when exposed to RvD1-device followed by TNF- α .

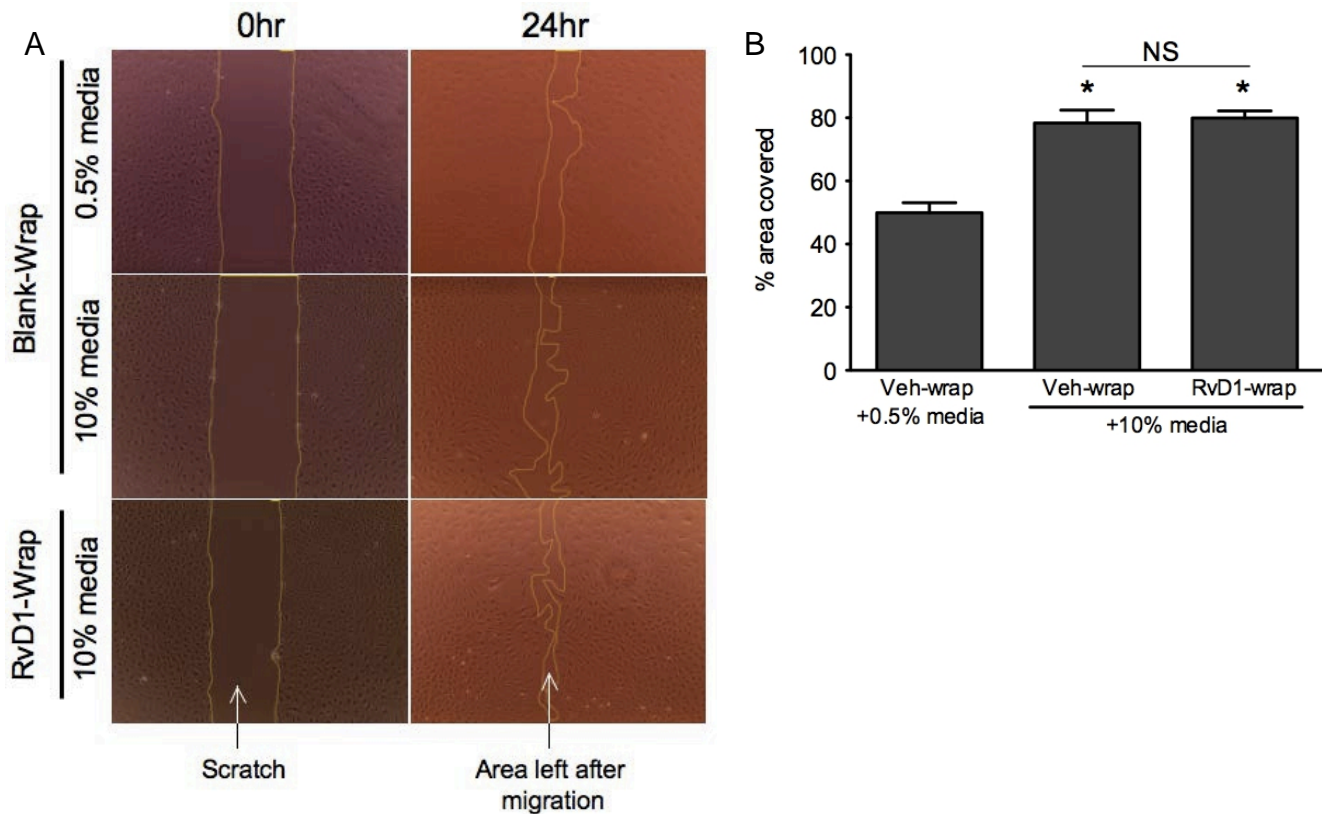


Figure 4.7 RvD1 eluting devices do not inhibit endothelial wound closure. Confluent human saphenous vein endothelial cells were starved overnight in media with 0.5% serum and induced to migrate in the scratched area with 10% serum containing media with a vehicle- or RvD1-device placed in transwell for 24 hours. Endothelial cells exposed to media with 0.5% serum and vehicle-loaded device served as the negative control without any migratory stimulus. (A) Representative images at 0 hour and 24 hour. Yellow line represents edge of the scratch. (B) Quantitative analysis of % area migrated in the scratched surface. N=8 per group except Control where N=4. N represents each well of a 24-well plate. * = $p < 0.05$ from vehicle wrap controls; NS: Not significant ($p > 0.05$).

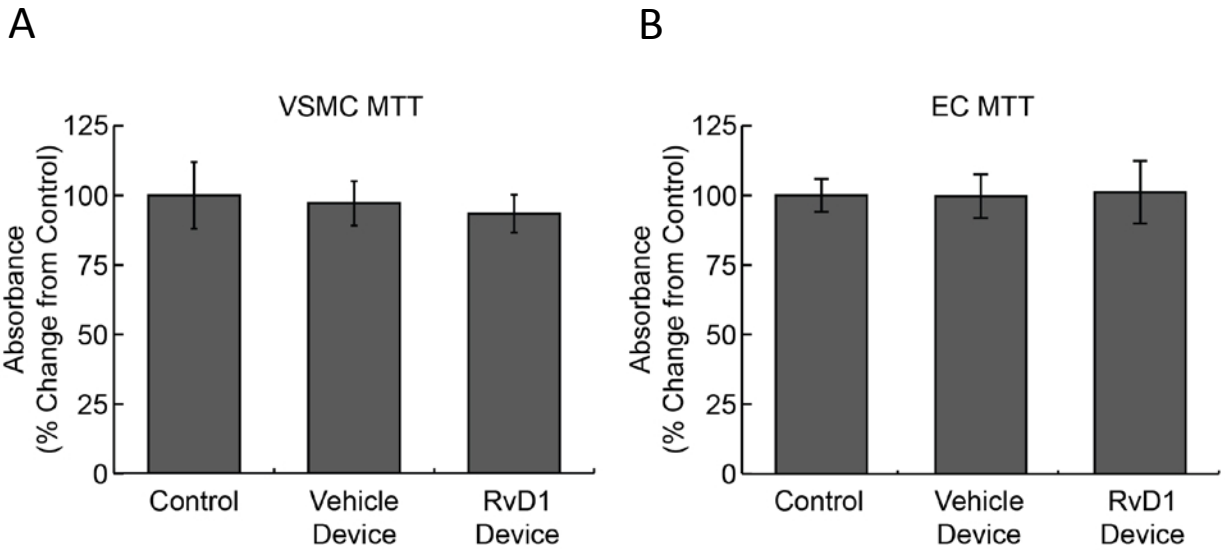


Figure 4.8 MTT cytotoxicity assay on (A) primary human vascular smooth muscle cells (VSMCs) and (B) endothelial cells (ECs) using trilayered PLGA devices (85:15 PLGA / 100ng RvD1 / 75:25 PLGA / 100ng RvD1 / 50:50 PLGA) and blank device (85:15 PLGA / Ethanol / 75:25 PLGA / Ethanol / 50:50 PLGA). Cells were grown to confluency in 24-well plates and were incubated for 24 hours with PLGA wraps placed on transwells. The wraps were removed after 24 hours and MTT assay was performed.

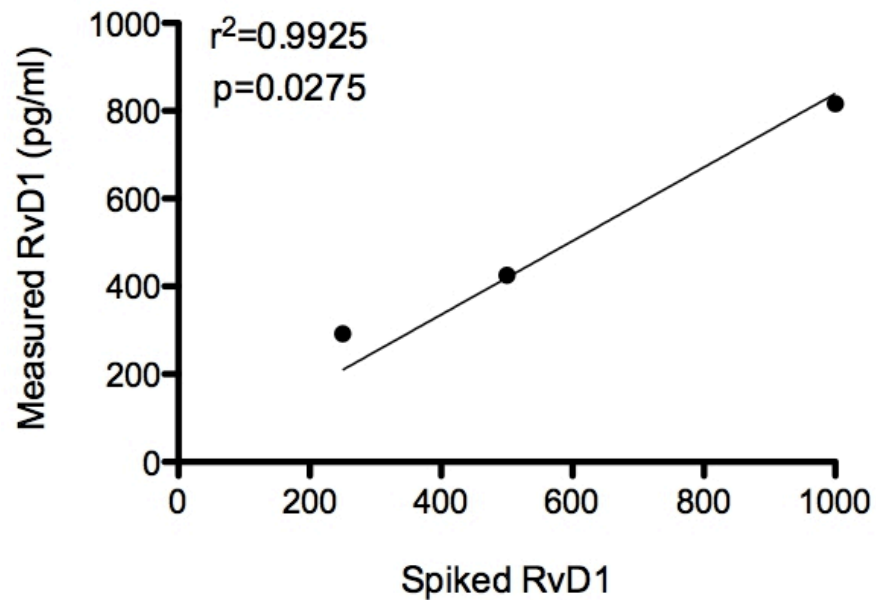


Figure 4.9 Linearity and detection of the EIA method for RvD1 measurement in rabbit vessels. Rabbit aortic segments were spiked with increasing amounts of authentic RvD1 and subjected to dounce homogenization and centrifugation through 30-KD filtration device and were analyzed for RvD1 levels.

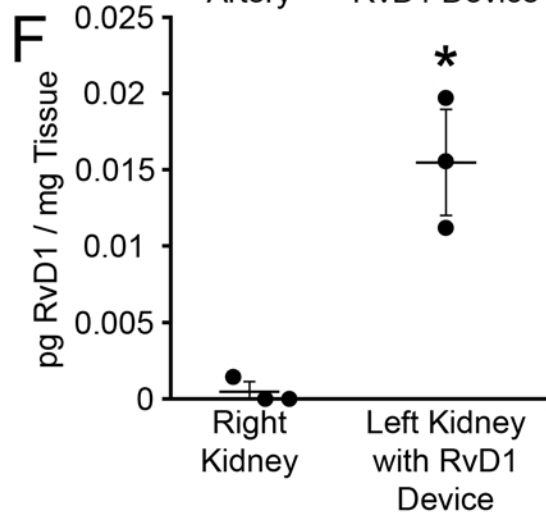
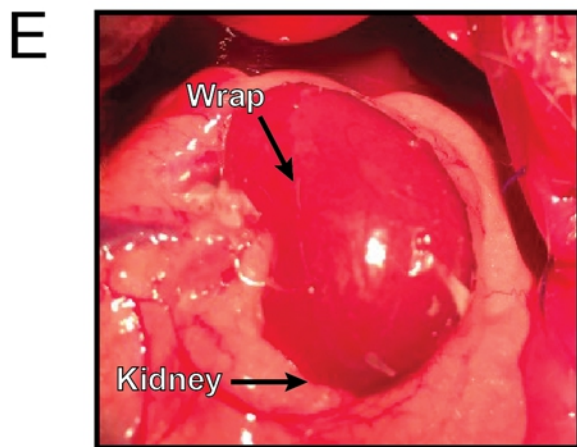
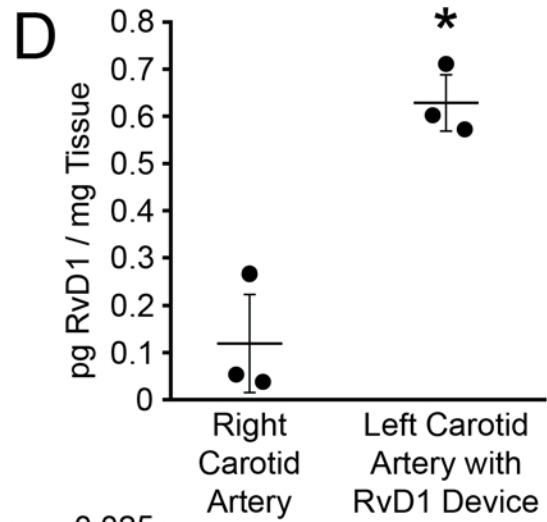
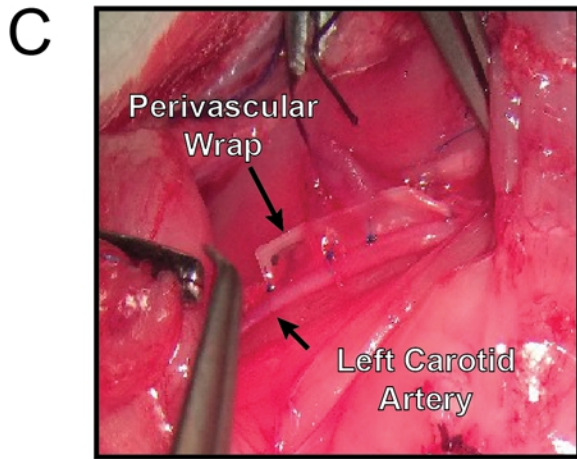
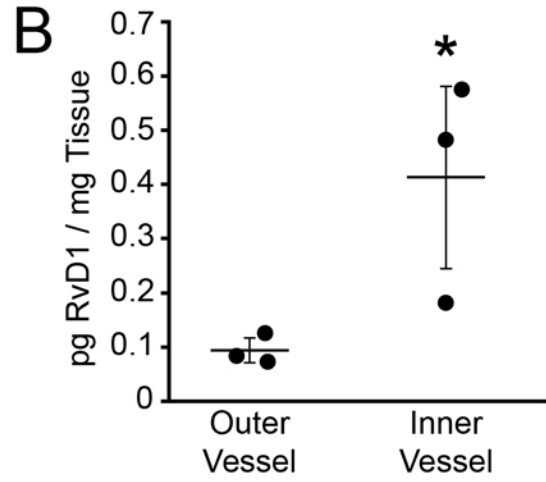
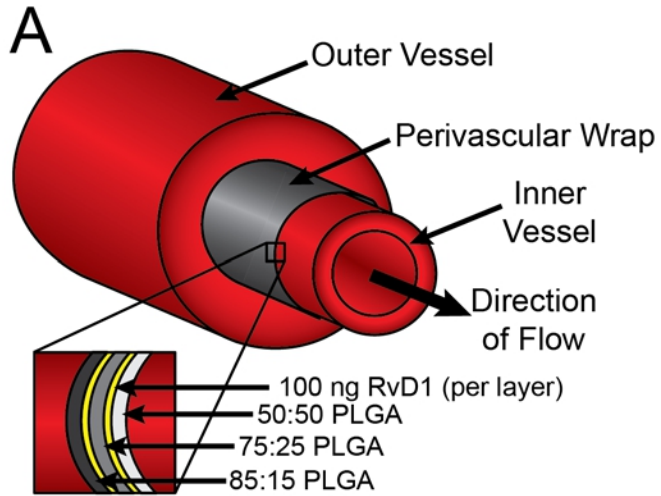


Figure 4.10 Unidirectional release of RvD1 from trilayered 85:15 PLGA / 100ng RvD1 / 75:25 PLGA / 100ng RvD1 / 50:50 PLGA devices. (A) Schematic diagram of an *ex vivo* closed-circuit flow system. An inner vessel (rabbit abdominal aorta) was secured and sealed to a flow chamber with regular DMEM media used to generate pulsatile flow at physiologic pressures supplied by an external pump. The trilayered wrap was then secured to the vessel with the 50:50 PLGA side facing inwards. A second vessel (rabbit thoracic aorta) was secured around the wrap and VSMC media was placed in the chamber surrounding the vessels and the system was allowed to run for 24hr at room temperature. (C, E) *In vivo* images of a trilayered device (C) secured around the left carotid artery or (E) placed on top of the left kidney in rats. (B, D, F) Net RvD1 uptake by the *ex vivo* vessels, carotid arteries, and kidneys as measured by EIA (n=3). *: $p \leq 0.05$ compared to blank wrap controls.

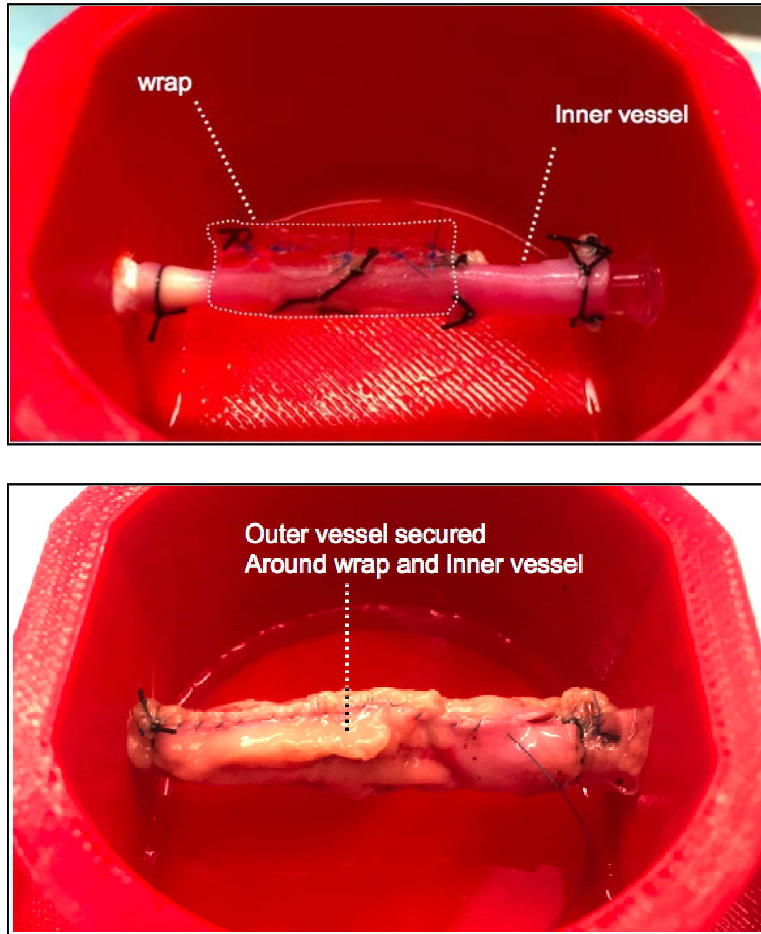


Figure 4.11 Ex-vivo flow chamber setup showing assembly of blood vessels with the wrap.

Chapter 5 – Summary and Conclusions

Polymer thin films hold great potential for the field of controlled drug delivery. The ability to tailor the properties of the polymer films to suit delivery of different drug classes to various sites in the body enables a wealth of potential solutions for improved disease treatment. The ability to tune the size, microstructure, and degradation of polymer film devices enables a variety of device types that can match the pharmacokinetic needs to best counteract the disease being treated. The polymer thin film devices discussed in this dissertation cover large and small molecule therapeutics, delivered to both the eye and the peripheral vasculature over days, months, and years.

The potential for PCL to release therapeutic in the eye over the many months of its degradation lifespan represents one pathway to treatment of chronic and blinding eye conditions, such as the treatments for neovascular age-related macular degeneration and uveitis discussed in chapters 2 and 3 of this dissertation. By eliminating the need for frequent injections, implantable sustained drug delivery devices can offer sustained drug concentrations at their site of action, without the need for monthly intraocular injections. A change from monthly injections to yearly injections holds the potential to improve patient compliance and outcomes, decrease physician workload, and reduce the burden of the cost of care on insurance companies.

PLGA thin films hold promise for the delivery of therapeutics to tissues following surgery. In this dissertation we presented a thin film wrap that releases a specialized pro-resolving mediator RvD1 with the aim of attenuating inflammation following peripheral vascular surgery or solid organ transplantation. PLGA thin films demonstrated their ability to release RvD1 unidirectionally over two weeks, degrade in a manner of weeks, and deliver detectable

levels of RvD1 into the target tissue. Together these features of PLGA thin films show the potential for the films in delivering SPMs following surgery.

Further work is required to advance the development of polymer thin film devices before they are able to reach the patient bedside. Most importantly, what has been shown in this dissertation is the ability for polymer thin film devices to deliver drug for a sustained period of time, what is needed next is a demonstration of an improvement in outcomes resulting from the increased and lasting drug concentrations. A positive effect on disease outcomes is the necessary piece of evidence to advance the need for sustained drug delivery for each disease. A second area for future work is the manufacturability of the polymer thin film devices. Currently every device is made by hand at the lab benchtop. Thin film device fabrication will have to be improved to allow for the manufacturing volume and quality standards needed for human use. Finally, for these devices there remains a need to demonstrate drug stability over long periods of time of storage and use. Improved drug formulations will need to be developed to maintain the potency of drugs over time, both on the shelf and in the body.

The field of controlled drug delivery holds great promise for advancing the treatment of disease, and polymer thin film devices represent an exciting area in that field. Given the potential for large drug payloads, long release time, excellent biocompatibility, and complete device degradation, there remains a tremendous potential for future development of more polymer thin film drug delivery devices in more disease areas and for even more therapeutic molecules.

References

1. Dash, T. K. & Konkimalla, V. B. Poly-ε-caprolactone based formulations for drug delivery and tissue engineering: A review. *J. Control. Release* **158**, 15–33 (2012).
2. Bernards, D. A. & Desai, T. A. Nanotemplating of biodegradable polymer membranes for constant-rate drug delivery. *Adv. Mater.* **22**, 2358–62 (2010).
3. Bernards, D. A., Lance, K. D., Ciaccio, N. A. & Desai, T. A. Nanostructured thin film polymer devices for constant-rate protein delivery. *Nano Lett.* **12**, 5355–61 (2012).
4. Bernards, D. A. *et al.* Ocular Biocompatibility and Structural Integrity of Micro- and Nanostructured Poly(caprolactone) Films. *J. Ocul. Pharmacol. Ther.* **29**, 249–57 (2013).
5. Makadia, H. K. & Siegel, S. J. Poly Lactic-co-Glycolic Acid (PLGA) as Biodegradable Controlled Drug Delivery Carrier. *Polymers (Basel)*. **3**, 1377–1397 (2011).
6. Anderson, J. M. & Shive, M. S. Biodegradation and biocompatibility of PLA and PLGA microspheres. *Adv. Drug Deliv. Rev.* **64**, 72–82 (2012).
7. Klose, D., Siepmann, F., Elkharraz, K. & Siepmann, J. PLGA-based drug delivery systems: importance of the type of drug and device geometry. *Int. J. Pharm.* **354**, 95–103 (2008).
8. NEI. Facts About Age-Related Macular Degeneration. at <https://nei.nih.gov/health/maculardegen/armd_facts>
9. de Jong, P. T. V. M. Age-related macular degeneration. *N. Engl. J. Med.* 1474–1485 (2006). at <<http://books.google.com/books?hl=en&lr=&id=HEz-SzdT2c8C&oi=fnd&pg=PA7&dq=Age-Related+Macular+Degeneration&ots=cKdNGSSyx6&sig=NJjOe5UHGMpUfLj5ots4XEk898g>>
10. Rosenfeld, P. J. *et al.* Ranibizumab for neovascular age-related macular degeneration. *N. Engl. J. Med.* **355**, 1419–1431 (2006).
11. Brown, D. M. *et al.* Ranibizumab versus Verteporfin Photodynamic Therapy for Neovascular Age-Related Macular Degeneration: Two-Year Results of the ANCHOR Study. *Ophthalmology* **116**, 57–65.e5 (2009).

12. Regillo, C. D. *et al.* Randomized, Double-Masked, Sham-Controlled Trial of Ranibizumab for Neovascular Age-related Macular Degeneration: PIER Study Year 1. *Am. J. Ophthalmol.* **145**, 239–248.e5 (2008).
13. Inc., P. I. for L. (Ranibizumab) G. Prescribing Information for Lucentis® (Ranibizumab). (2006).
14. Campochiaro, P. a. *et al.* Monthly Versus As-Needed Ranibizumab Injections in Patients with Retinal Vein Occlusion. The SHORE Study. *Ophthalmology* **121**, 1–11 (2014).
15. Busbee, B. G. *et al.* Twelve-month efficacy and safety of 0.5 mg or 2.0 mg ranibizumab in patients with subfoveal neovascular age-related macular degeneration. *Ophthalmology* **120**, 1046–56 (2013).
16. Suhler, E. B., Lloyd, M. J., Choi, D., Rosenbaum, J. T. & Austin, D. F. Incidence and prevalence of uveitis in Veterans Affairs Medical Centers of the Pacific Northwest. *Am. J. Ophthalmol.* **146**, 890–6.e8 (2008).
17. Suttorp-Schulten, M. S. & Rothova, a. The possible impact of uveitis in blindness: a literature survey. *Br. J. Ophthalmol.* **80**, 844–848 (1996).
18. Pato, E. *et al.* Systematic review on the effectiveness of immunosuppressants and biological therapies in the treatment of autoimmune posterior uveitis. *Semin. Arthritis Rheum.* **40**, 314–23 (2011).
19. Hazirolan, D. & Pleyer, U. Think Global - Act Local: Intravitreal Drug Delivery Systems in Chronic Noninfectious Uveitis. *Ophthalmic Res.* **49**, 59–65 (2012).
20. Nguyen, Q. D. *et al.* Ocular tolerability and efficacy of intravitreal and subconjunctival injections of sirolimus in patients with non-infectious uveitis: primary 6-month results of the SAVE Study. *J. Ophthalmic Inflamm. Infect.* **3**, 32 (2013).
21. Serhan, C. N. Pro-resolving lipid mediators are leads for resolution physiology. *Nature* **510**, 92–101 (2014).
22. Akagi, D., Chen, M., Toy, R., Chatterjee, a. & Conte, M. S. Systemic delivery of proresolving lipid mediators resolvin D2 and maresin 1 attenuates intimal hyperplasia in mice. *FASEB J.* **29**, 2504–2513 (2015).

23. Miyahara, T. *et al.* D-series resolvins attenuates vascular smooth muscle cell activation and neointimal hyperplasia following vascular injury. *FASEB J.* **27**, 2220–2232 (2013).
24. Lu, L., Garcia, C. a & Mikos, a G. In vitro degradation of thin poly(DL-lactic-co-glycolic acid) films. *J. Biomed. Mater. Res.* **46**, 236–44 (1999).
25. Morath, C. *et al.* Sirolimus in renal transplantation. *Nephrol. Dial. Transplant* **22 Suppl 8**, viii61–viii65 (2007).
26. Puranik, A. S., Dawson, E. R. & Peppas, N. a. Recent advances in drug eluting stents. *Int. J. Pharm.* **441**, 665–79 (2013).
27. Dasari, T. W., Patel, B. & Saucedo, J. F. Systematic review of effectiveness of oral sirolimus after bare-metal stenting of coronary arteries for prevention of in-stent restenosis. *Am. J. Cardiol.* **112**, 1322–7 (2013).
28. Shanmuganathan, V. A. *et al.* The efficacy of sirolimus in the treatment of patients with refractory uveitis. *Br. J. Ophthalmol.* **89**, 666–9 (2005).
29. Phillips, B. N. & Wroblewski, K. J. A retrospective review of oral low-dose sirolimus (rapamycin) for the treatment of active uveitis. *J. Ophthalmic Inflamm. Infect.* **1**, 29–34 (2011).
30. Mudumba, S. *et al.* Tolerability and Pharmacokinetics of Intravitreal Sirolimus. *J. Ocul. Pharmacol. Ther.* **28**, 507–514 (2012).
31. Study Assessing Double-masked Uveitis Treatment (SAKURA). at <<http://clinicaltrials.gov/show/NCT01358266>>
32. Nieto, a. *et al.* Surface Engineering of Porous Silicon Microparticles for Intravitreal Sustained Delivery of Rapamycin. *Invest. Ophthalmol. Vis. Sci.* **56**, 1070–1080 (2015).
33. Hou, H. *et al.* A sustained intravitreal drug delivery system with remote real time monitoring capability. *Acta Biomater.* (2015). doi:10.1016/j.actbio.2015.06.012
34. Cholkar, K., Gunda, S., Earla, R., Pal, D. & Mitra, A. K. Nanomicellar Topical Aqueous Drop Formulation of Rapamycin for Back-of-the-Eye Delivery. *AAPS PharmSciTech*

(2014). doi:10.1208/s12249-014-0244-2

35. Heiligenhaus, A. *et al.* Everolimus for the treatment of uveitis refractory to cyclosporine A: a pilot study. *Graefes Arch. Clin. Exp. Ophthalmol.* **251**, 143–52 (2013).
36. Kholdebarin, R., Campbell, R. J., Jin, Y.-P. & Buys, Y. M. Multicenter study of compliance and drop administration in glaucoma. *Can. J. Ophthalmol. / J. Can. d'Ophthalmologie* **43**, 454–461 (2008).
37. Edelhauser, H. F. *et al.* Ophthalmic drug delivery systems for the treatment of retinal diseases: basic research to clinical applications. *Invest. Ophthalmol. Vis. Sci.* **51**, 5403–20 (2010).
38. Tempest-Roe, S., Joshi, L., Dick, A. D. & Taylor, S. R. Local therapies for inflammatory eye disease in translation: past, present and future. *BMC Ophthalmol.* **13**, 39 (2013).
39. Silva-Cunha, A., Fialho, S. L., Naud, M.-C. & Behar-Cohen, F. Poly- ϵ -Caprolactone Intravitreal Devices: An In Vivo Study. *Investig. Ophthalmology Vis. Sci.* **50**, 2312 (2009).
40. Sun, H., Mei, L., Song, C., Cui, X. & Wang, P. The in vivo degradation, absorption and excretion of PCL-based implant. *Biomaterials* **27**, 1735–40 (2006).
41. Natu, M. V., de Sousa, H. C. & Gil, M. H. Influence of polymer processing technique on long term degradation of poly(ϵ -caprolactone) constructs. *Polym. Degrad. Stab.* **98**, 44–51 (2013).
42. Kim, M.-S. *et al.* Enhanced bioavailability of sirolimus via preparation of solid dispersion nanoparticles using a supercritical antisolvent process. *Int. J. Nanomedicine* **6**, 2997–3009 (2011).
43. Il'ichev, Y., Alquier, L. & Maryanoff, C. Degradation of rapamycin and its ring-opened isomer: role of base catalysis. *ARKIVOC* **xii**, 110–131 (2007).
44. Carvalho, S. R. *et al.* Characterization and pharmacokinetic analysis of crystalline versus amorphous rapamycin dry powder via pulmonary administration in rats. *Eur. J. Pharm. Biopharm.* **88**, 136–147 (2014).
45. Schwartz, G. F. Compliance and persistency in glaucoma follow-up treatment. *Curr.*

- Opin. Ophthalmol.* **16**, 114–121 (2005).
46. Reardon, G., Kotak, S. & Schwartz, G. F. Objective assessment of compliance and persistence among patients treated for glaucoma and ocular hypertension: a systematic review. *Patient Prefer. Adherence* **5**, 441–63 (2011).
 47. Ranta, V.-P. *et al.* Barrier analysis of periocular drug delivery to the posterior segment. *J. Control. Release* **148**, 42–48 (2010).
 48. Boddu, S. H., Gupta, H. & Patel, S. Drug Delivery to the Back of the Eye Following Topical Administration: An Update on Research and Patenting Activity. *Recent Pat. Drug Deliv. Formul.* 27–36 (2014). doi:10.2174/1872211308666140130093301
 49. Maurice, D. M. Drug Delivery to the Posterior Segment : An Update. *Retin. Today* **47**, (2013).
 50. The CATT Research Group. Ranibizumab and bevacizumab for neovascular age-related macular degeneration. *N. Engl. J. Med.* **364**, 1897–1908 (2011).
 51. Heier, J. S. *et al.* Intravitreal aflibercept (VEGF trap-eye) in wet age-related macular degeneration. *Ophthalmology* **119**, 2537–2548 (2012).
 52. Varma, R. *et al.* Improved vision-related function after ranibizumab for macular edema after retinal vein occlusion: Results from the BRAVO and CRUISE trials. *Ophthalmology* **119**, 2108–2118 (2012).
 53. Nguyen, Q. D. *et al.* Ranibizumab for Diabetic Macular Edema. *Ophthalmology* **119**, 789–801 (2012).
 54. Ghasemi Falavarjani, K. & Nguyen, Q. D. Adverse events and complications associated with intravitreal injection of anti-VEGF agents: a review of literature. *Eye* **27**, 787–794 (2013).
 55. Townsend, D. *et al.* Health professionals' and service users' perspectives of shared care for monitoring wet age-related macular degeneration: a qualitative study alongside the ECHoES trial. *BMJ Open* **5**, e007400 (2015).
 56. Amoaku, W. *et al.* Action on AMD. Optimising patient management: act now to ensure current and continual delivery of best possible patient care. *Eye (Lond)*. **26 Suppl 1**, S2–

- 21 (2012).
57. Rawas-Qalaji, M. & Williams, C.-A. Advances in ocular drug delivery. *Curr. Eye Res.* **37**, 345–56 (2012).
 58. Kuno, B. N. & Fujii, S. Ocular Drug Delivery Systems for the Posterior Segment : A Review. *Retin. Today* (2012).
 59. Kang-Mieler, J. J., Osswald, C. R. & Mieler, W. F. Advances in ocular drug delivery: emphasis on the posterior segment. *Expert Opin. Drug Deliv.* **5247**, 1–14 (2014).
 60. Kane, F. E., Burdan, J., Cutino, A. & Green, K. E. Iluvien: a new sustained delivery technology for posterior eye disease. *Expert Opin. Drug Deliv.* **5**, 1039–1046 (2008).
 61. Kuppermann, B. D. *et al.* Randomized controlled study of an intravitreal dexamethasone drug delivery system in patients with persistent macular edema. *Arch. Ophthalmol.* **125**, 309 – 317 (2007).
 62. Bhagat, R., Zhang, J., Farooq, S. & Li, X.-Y. Comparison of the Release Profile and Pharmacokinetics of Intact and Fragmented Dexamethasone Intravitreal Implants in Rabbit Eyes. *J. Ocul. Pharmacol. Ther.* **30**, 854–858 (2014).
 63. Pardo-López, D., Francés-Muñoz, E., Gallego-Pinazo, R. & Díaz-Llopis, M. Anterior chamber migration of dexamethasone intravitreal implant (Ozurdex®). *Graefe's Arch. Clin. Exp. Ophthalmol.* **250**, 1703–1704 (2012).
 64. Vela, J. I., Crespí, J. & Andreu, D. Repositioning of dexamethasone intravitreal implant (Ozurdex®) migrated into the anterior chamber. *Int. Ophthalmol.* **32**, 583–584 (2012).
 65. Wai Ch'ng, S., Padroni, S. & Banerjee, S. Anterior vitreous displacement of the intravitreal dexamethasone implant (Ozurdex). *Eye (Lond)*. **28**, 238–9 (2014).
 66. Kim, Y. C., Chiang, B., Wu, X. & Prausnitz, M. R. Ocular delivery of macromolecules. *J. Control. Release* **190**, 172–181 (2014).
 67. Taluja, A., Youn, Y. S. & Bae, Y. H. Novel approaches in microparticulate PLGA delivery systems encapsulating proteins. *J. Mater. Chem.* **17**, 4002 (2007).

68. Sinha, V. R. & Trehan, A. Biodegradable microspheres for protein delivery. *J. Control. Release* **90**, 261–80 (2003).
69. Nadarassan, D. K. Sustained Release of Bevacizumab (Avastin) from BioSilicon. *Invest. Ophthalmol. Vis. Sci.* **55**, 1950 (2014).
70. Owens, G. *et al.* Establishing In Vivo to In Vitro Correlations for the Rate of Release of Bevacizumab from Extended Release Formulations. *Invest. Ophthalmol. Vis. Sci.* **56**, 236 (2015).
71. Rubio, R. G. Long-Acting Anti-VEGF Delivery. *Retin. Today* 78–80 (2014).
72. Gaudreault, J. *et al.* Pharmacokinetics and retinal distribution of ranibizumab, a humanized antibody fragment directed against VEGF-A, following intravitreal administration in rabbits. *Retina* **27**, 1260 (2007).
73. Missel, P. J. Simulating intravitreal injections in anatomically accurate models for rabbit, monkey, and human eyes. *Pharm. Res.* **29**, 3251–3272 (2012).
74. Gaudreault, J. *et al.* Pharmacokinetics and retinal distribution of ranibizumab, a humanized antibody fragment directed against VEGF-A, following intravitreal administration in rabbits. *Retina* **27**, 1260–6 (2003).
75. Vézina, M. in *Assessing Ocular Toxicology in Laboratory Animals* (eds. Weir, A. B. & Collins, M.) 1–21 (Humana Press, 2013). doi:10.1007/978-1-62703-164-6
76. Weylandt, K. H., Kang, J. X., Wiedenmann, B. & Baumgart, D. C. Lipoxins and resolvins in inflammatory bowel disease. *Inflamm. Bowel Dis.* **13**, 797–799 (2007).
77. Bento, A. F., Claudino, R. F., Dutra, R. C., Marcon, R. & Calixto, J. B. Omega-3 fatty acid-derived mediators 17(R)-hydroxy docosahexaenoic acid, aspirin-triggered resolvin D1 and resolvin D2 prevent experimental colitis in mice. *J. Immunol.* **187**, 1957–1969 (2011).
78. Spite, M. *et al.* Resolvin D2 is a potent regulator of leukocytes and controls microbial sepsis. *Nature* **461**, 1287–1291 (2009).
79. Wang, B. *et al.* Resolvin D1 protects mice from LPS-induced acute lung injury. *Pulm. Pharmacol. Ther.* **24**, 434–441 (2011).

80. Duffield, J. S. *et al.* Resolvin D series and protectin D1 mitigate acute kidney injury. *J. Immunol.* **177**, 5902–5911 (2006).
81. Fredman, G. *et al.* Impaired phagocytosis in localized aggressive periodontitis: Rescue by resolvin E1. *PLoS One* **6**, (2011).
82. Fredman, G. & Serhan, C. N. Specialized proresolving mediator targets for RvE1 and RvD1 in peripheral blood and mechanisms of resolution. *Biochem. J.* **437**, 185–197 (2011).
83. Serhan, C. N. & Chiang, N. Resolution phase lipid mediators of inflammation: Agonists of resolution. *Curr. Opin. Pharmacol.* **13**, 632–640 (2013).
84. Lee, C. H. Resolvins as new fascinating drug candidates for inflammatory diseases. *Arch. Pharm. Res.* **35**, 3–7 (2012).
85. Campbell, E. L. *et al.* Resolvin E1 promotes mucosal surface clearance of neutrophils: a new paradigm for inflammatory resolution. *FASEB J.* **21**, 3162–3170 (2007).
86. Chiang, N. *et al.* Infection regulates pro-resolving mediators that lower antibiotic requirements. *Nature* **484**, 524–528 (2012).
87. Fullerton, J. N., O'Brien, A. J. & Gilroy, D. W. Lipid mediators in immune dysfunction after severe inflammation. *Trends Immunol.* **35**, 12–21 (2014).
88. Kasuga, K. *et al.* Rapid appearance of resolvin precursors in inflammatory exudates: novel mechanisms in resolution. *J. Immunol.* **181**, 8677–8687 (2008).
89. Pires, N. M. M. *et al.* Local perivascular delivery of anti-restenotic agents from a drug-eluting poly(epsilon-caprolactone) stent cuff. *Biomaterials* **26**, 5386–94 (2005).
90. Yu, X. *et al.* A rapamycin-releasing perivascular polymeric sheath produces highly effective inhibition of intimal hyperplasia. *J. Control. Release* **191**, 47–53 (2014).
91. Kohler, T. R., Toleikis, P. M., Gravett, D. M. & Avelar, R. L. Inhibition of neointimal hyperplasia in a sheep model of dialysis access failure with the bioabsorbable Vascular Wrap paclitaxel-eluting mesh. *J. Vasc. Surg.* **45**, 1029–1037; discussion 1037–8 (2007).


92. Signore, P. E. *et al.* Complete inhibition of intimal hyperplasia by perivascular delivery of paclitaxel in balloon-injured rat carotid arteries. *J Vasc Interv Radiol* **12**, 79–88 (2001).
93. Kanjickal, D., Lopina, S., Evancho-Chapman, M. M., Schmidt, S. & Donovan, D. Sustained local drug delivery from a novel polymeric ring to inhibit intimal hyperplasia. *J. Biomed. Mater. Res. A* **93**, 656–65 (2010).
94. Sanders, W. G., Hoglebe, P. C., Grainger, D. W., Cheung, A. K. & Terry, C. M. A biodegradable perivascular wrap for controlled, local and directed drug delivery. *J. Control. Release* **161**, 81–9 (2012).
95. Colas, R. A., Shinohara, M., Dalli, J., Chiang, N. & Serhan, C. N. Identification and signature profiles for pro-resolving and inflammatory lipid mediators in human tissue. *Am J Physiol Cell Physiol* **307**, C39–C54 (2014).
96. Dalli, J. & Serhan, C. N. Specific lipid mediator signatures of human phagocytes: Microparticles stimulate macrophage efferocytosis and pro-resolving mediators. *Blood* **120**, 60–73 (2012).
97. Chatterjee, A. *et al.* The Pro-Resolving Lipid Mediator Maresin 1 (MaR1) Attenuates Inflammatory Signaling Pathways in Vascular Smooth Muscle and Endothelial Cells. *PLoS One* **9**, e113480 (2014).
98. Chen, D. *et al.* Robust and flexible free-standing films for unidirectional drug delivery. *Langmuir* **29**, 8328–34 (2013).
99. Vasconcelos, D. P. *et al.* Development of an immunomodulatory biomaterial: Using resolvin D1 to modulate inflammation. *Biomaterials* **53**, 566–573 (2015).
100. Norling, L. V *et al.* Cutting edge: Humanized nano-proresolving medicines mimic inflammation-resolution and enhance wound healing. *J. Immunol.* **186**, 5543–5547 (2011).
101. Chen, J. *et al.* Aspirin-triggered resolvin D1 down-regulates inflammatory responses and protects against endotoxin-induced acute kidney injury. *Toxicol. Appl. Pharmacol.* **277**, 118–123 (2014).

Publishing Agreement

It is the policy of the University to encourage the distribution of all theses, dissertations, and manuscripts. Copies of all UCSF theses, dissertations, and manuscripts will be routed to the library via the Graduate Division. The library will make all theses, dissertations, and manuscripts accessible to the public and will preserve these to the best of their abilities, in perpetuity.

Please sign the following statement:

I hereby grant permission to the Graduate Division of the University of California, San Francisco to release copies of my thesis, dissertation, or manuscript to the Campus Library to provide access and preservation, in whole or in part, in perpetuity.



Author Signature



Date